isvr Institute of Sound and Vibration Research

Active Control of Structural Vibration Transmission between Two Plates Connected by a Set of Active Mounts

P. Gardonio and S.J. Elliott

ISVR Technical Memorandum 834

January 1999

University of Southampton

SCIENTIFIC PUBLICATIONS BY THE ISVR

Technical Reports are published to promote timely dissemination of research results by ISVR personnel. This medium permits more detailed presentation than is usually acceptable for scientific journals. Responsibility for both the content and any opinions expressed rests entirely with the author(s).

Technical Memoranda are produced to enable the early or preliminary release of information by ISVR personnel where such release is deemed to the appropriate. Information contained in these memoranda may be incomplete, or form part of a continuing programme; this should be borne in mind when using or quoting from these documents.

Contract Reports are produced to record the results of scientific work carried out for sponsors, under contract. The ISVR treats these reports as confidential to sponsors and does not make them available for general circulation. Individual sponsors may, however, authorize subsequent release of the material.

UNIVERSITY OF SOUTHAMPTON

INSTITUTE OF SOUND AND VIBRATION RESEARCH

SIGNAL PROCESSING AND CONTROL GROUP

Active Control of Structural Vibration Transmission Between Two Plates Connected by a Set of Active Mounts

by

P. Gardonio and S.J. Elliott

ISVR Technical Memorandum No. 834

January 1999

Authorized for issue by
Professor S.J. Elliott
Group Chairman

ABSTRACT

This report presents the results of the research activity carried out at ISVR within a collaborative program whose acronym is AIRAT: "Active Isolator Research for Aircraft Trim Panels". The main goal of the project is to study and develop an active mounting system for the trim panels mounted in aircraft or helicopter in order to reduce the sound transmission to the cabin.

This report introduces the theory of an impedance-mobility matrix model used to predict the structural vibration transmission between two plates which are mechanically coupled via an active mounting system but are acoustically uncoupled. With this model the active and passive isolation effectiveness of different types of mounting systems have been studied. In particular, the case of a single or a three mount isolator system with inertial or reactive actuators has been investigated in order to assess the effects generated by the mounts stiffnesses and the effects produced by the rigid elements (block masses) present at each end of the mounts.

Three cost functions have been investigated: first, the minimisation of the total structural power transmitted by the source to the receiver; second, the cancellation of out-of-plane input velocities to the receiver and third the cancellation of out-of-plane input forces to the receiver.

The simulations carried out have shown that the best passive and active isolation are both achieved when soft mounts are used. The number of mounts and the presence of block masses at each end of the mounts significantly affect the passive isolation but have shown smaller influence on the active isolation. The three control strategies studied have shown similar active control effectiveness in all cases examined and for both inertial or reactive control actuators.

Finally, the impedance-mobility matrix model used and described in this report has been validated with data given by other theoretical and experimental analysis carried out on a two plate system with a three aluminium or rubber active mounting system.

INDEX

1. INTRODUCTION

The work summarised in this report forms part of a collaborative research program called AIRAT[1] which aims to reduce the structure-borne and air-borne sound transmission through the double wall structure of aircraft or helicopters. The goal of the project is to develop an active mounting system for trim panels covering the fuselage structure (frames and fuselage skin) in order to reduce the structure-borne and air-borne sound transmission and radiation into the cabin by the trims themselves. This report deals specifically with the theoretical analysis of structural vibration transmission through an active mounting system that connects two plates acoustically uncoupled.

The problem of structure-borne noise transmission between flexible mechanical systems connected via a set of mounts cannot be studied using the standard mathematical models given in reference books which considers the mounting system as a single lumped spring in parallel with a damper [1]. A more detailed model is needed which accounts for the effects of multiple mounts and for the effects of multiple degrees of freedom vibration transmission at the connecting points. Also, the distributed nature of the source and receiver structures and some isolator components has to be accounted for so that coupling effects between the vibration components related to different types of waves propagating on the three system's elements is accounted.

The Finite Element Method, FEM [2], could be employed for this type of study but it generates large matrix models that require very long simulations for a relatively small frequency range of analysis, even when the latest personal computer or work stations available on the market are used. Two alternative approaches are more suitable for structure-borne noise transmission problems at audio frequencies. The first one is the Statistical Energy Analysis approach, SEA [3]. This approach is based on power transmission concepts using coupling factors between a source and receiver structures assuming the two structures of either infinite or semi-infinite extend. This simplification allows the prediction of the vibration level of the source and receiver structures with a relatively simple matrix model that could be utilised up to high frequencies (several kHz) with relatively fast computer simulations. The simplification introduced by the SEA approach of neglecting the resonant effect of the source and receiver structures could lead to some problems in the so called low-mid frequency range between about 0 and 1 kHz, particularly if the effects of active control devices such as an active mounting system are under study. The second approach based on Impedances and Mobilities Matrices IMM has therefore been employed by ISVR in the AIRAT project so that the resonant behaviour of the three elements and the multiple degrees of freedom vibration transmission at the elements junctions can be accounted for in the calculations with a relatively simple matrix model.

Both, the SEA and IMM approaches have been used in the AIRAT project so that two tools were available for the understanding of the passive and active isolation effects produced by the mounting system studied and developed in the project. In this report the simulations carried out with a matrix model based on point and transfer mobilities or impedances is presented [4]. This model considers the system divided into three elements: the source, the mounting system and the receiver. These elements are assumed to be connected at a finite number of point junctions at which multi-degrees-of-freedom vibration transmission occurs. The three elements are modelled as distributed one- or bi-dimensional systems on which structural waves can propagate. The mounts are modelled as passive rubber element with either a reactive or an inertial control actuator which have been

[1] Active Isolator Research for Aircraft Trim Panels: "AIRAT".

represented respectively by a pair of reactive forces applied at each mount end or by a sky hook control force applied at one end of the mounts. The effects of some parts of the mounting systems or of the source and receiver systems can also be included in the model as lumped masses, springs and dampers.

The vibration of the source and receiver system has been expressed in terms of kinetic energy. In particular, an estimate of the kinetic energy represented by the square values of the out of plane velocities at 5 points of the source and receiver plates has been used so that the estimate of kinetic energy derived from experimental measurements taken on those points can be compared with the results obtained with the simulations.

This mathematical model allows the study of different control strategies by considering the minimisation of a quadratic cost function. In particular the effect of cancelling either the axial velocity or axial force at the top of the mount control strategy has been compared with the optimal control approach of minimising the total power transmitted from the source to the receiver.

Two configurations of the mounting system have been studied: the first considers a single mount while the second considers three mounts aligned. The effects of the mounts stiffnesses and the effects of lumped masses applied at the mounts' ends has also been assessed.

Finally, a comparison between the results obtained here with those from an SEA method and those obtained from an experimental set up is presented.

2. MATRIX MODEL FOR AN ACTIVE ISOLATING SYSTEM

In references [5-18] different types of mathematical models are described for the study of isolator systems composed by a source of vibration, a transmitting system and a receiver structure. Each of these models consider in details some aspects of the vibration transmission. In this section it is described the mobility-impedance matrix model used to derive the steady state response to harmonic excitation of the isolator system considered in this report. With this model it is possible consider the following features of an isolator system: first, the effects due to flexible and distributed source, mounting and receiver structures; second, the effects generated by a multiple mounting isolator systems and third the multiple degrees-of-freedom vibration transmission at the junctions of each mount.

The complete isolating system is divided into three flexible parts as shown in figure 1: the source, the mounting system, composed of n elements, and the receiver. These parts are connected at a finite number of junctions. At each junction, the motion and the forces transmitted are characterised by six complex parameters at a single frequency of excitation which is characterised by a time dependence of the form $\exp(j\omega t)$. These velocity and force parameters are grouped in a velocity junction vector and a force junction vector which, for the j[th] junction can be written as

$$\mathbf{v}_j^T \equiv \left\{ \dot{u}_j \quad \dot{v}_j \quad \dot{w}_j \quad \dot{\theta}_{xj} \quad \dot{\theta}_{yj} \quad \dot{\theta}_{zj} \right\} \qquad \mathbf{f}_j^T \equiv \left\{ N_{xj} \quad N_{yj} \quad N_{zj} \quad M_{xj} \quad M_{yj} \quad M_{zj} \right\} \tag{1,2}$$

where $\dot{u}_j$, $\dot{v}_j$, $\dot{w}_j$ are the complex linear velocities respectively along the x, y and z directions, $\dot{\theta}_{xj}$, $\dot{\theta}_{yj}$, $\dot{\theta}_{zj}$ are the complex angular velocities referred respectively to the x, y and z axis, N_{xj}, N_{yj}, N_{zj} are the complex forces in the x, y and z directions and finally M_{xj}, M_{yj}, M_{zj} are the complex moments referred respectively to the x, y and z axis.

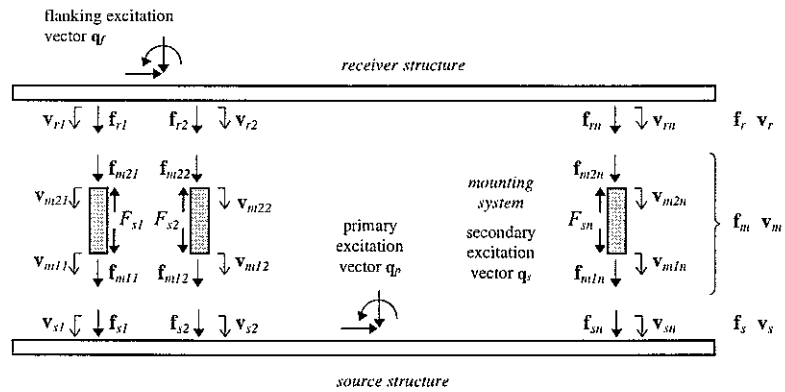

Fig. 1: *Scheme of a general complete isolating system.*

With reference to the notation shown in figure 1, combinations of these junction vectors are then grouped together to form three combined pairs of vectors: the source *velocity vector* ($\mathbf{v}_s$) and *force vector* ($\mathbf{f}_s$), the receiver *velocity vector* ($\mathbf{v}_r$) and *force vector* ($\mathbf{f}_r$) and the mounting system *velocity vector* ($\mathbf{v}_m$) and *force vector* ($\mathbf{f}_m$). The source and receiver velocity vector and force vector are given by:

$$\mathbf{v}_s \equiv \begin{Bmatrix} \mathbf{v}_{s1} \\ \mathbf{v}_{s2} \\ \vdots \\ \mathbf{v}_{sn} \end{Bmatrix} \qquad \mathbf{f}_s \equiv \begin{Bmatrix} \mathbf{f}_{s1} \\ \mathbf{f}_{s2} \\ \vdots \\ \mathbf{f}_{sn} \end{Bmatrix} \qquad \mathbf{v}_r \equiv \begin{Bmatrix} \mathbf{v}_{r1} \\ \mathbf{v}_{r2} \\ \vdots \\ \mathbf{v}_{rn} \end{Bmatrix} \qquad \mathbf{f}_r \equiv \begin{Bmatrix} \mathbf{f}_{r1} \\ \mathbf{f}_{r2} \\ \vdots \\ \mathbf{f}_{rn} \end{Bmatrix} \tag{3-6}$$

where $\mathbf{v}_{sj}$, $\mathbf{f}_{sj}$ represent the velocity junction vector and the force junction vector at the source junction for the j^{th} mount, while $\mathbf{v}_{rj}$, $\mathbf{f}_{rj}$ represent the velocity junction vector and the force junction vector at the receiver junction for the j^{th} mount. The vectors of velocities and forces of the mounting system are given by:

$$\mathbf{v}_m^T \equiv \left\{ \mathbf{v}_{m11}^T \quad \mathbf{v}_{m12}^T \quad \cdots \quad \mathbf{v}_{m1n}^T \quad \mathbf{v}_{m21}^T \quad \mathbf{v}_{m22}^T \quad \cdots \quad \mathbf{v}_{m2n}^T \right\} \tag{7}$$

$$\mathbf{f}_m^T \equiv \left\{ \mathbf{f}_{m11}^T \quad \mathbf{f}_{m12}^T \quad \cdots \quad \mathbf{f}_{m1n}^T \quad \mathbf{f}_{m21}^T \quad \mathbf{f}_{m22}^T \quad \cdots \quad \mathbf{f}_{m2n}^T \right\} \tag{8}$$

where $\mathbf{v}_{m1j}$, $\mathbf{f}_{m1j}$ represent the velocity junction vector and the force junction vector at the source junction for the j^{th} mount and $\mathbf{v}_{m2j}$, $\mathbf{f}_{m2j}$ represent the velocity junction vector and the force junction vector at the receiver junction for the j^{th} mount.

The dynamics of the source and the receiver are studied using a mobility matrix approach so that their velocity and force vectors can be written in the form:

$$\mathbf{v}_s = \mathbf{M}_{s1}\mathbf{f}_s + \mathbf{M}_{s2}\mathbf{q}_p \qquad\qquad \mathbf{v}_r = \mathbf{M}_{r1}\mathbf{f}_r + \mathbf{M}_{r2}\mathbf{q}_f \tag{9,10}$$

where $\mathbf{M}_{s1}$, $\mathbf{M}_{s2}$ and $\mathbf{M}_{r1}$, $\mathbf{M}_{r2}$ are mobility matrices respectively of the source and the receiver structures and $\mathbf{q}_p$, $\mathbf{q}_f$ are the primary excitation vector and the flanking excitation vectors

$$\mathbf{q}_p^T = \left\{ \mathbf{q}_{p1}^T \quad \mathbf{q}_{p2}^T \quad \cdots \quad \mathbf{q}_{pN}^T \right\} \qquad \mathbf{q}_f^T = \left\{ \mathbf{q}_{f1}^T \quad \mathbf{q}_{f2}^T \quad \cdots \quad \mathbf{q}_{fM}^T \right\} \tag{11,12}$$

with

$$\mathbf{q}_{pj}^T = \left\{ F_{xj} \quad F_{yj} \quad F_{zj} \quad T_{xj} \quad T_{yj} \quad T_{zj} \right\} \qquad \mathbf{q}_{fi}^T = \left\{ F_{xj} \quad F_{yj} \quad F_{zj} \quad T_{xj} \quad T_{yj} \quad T_{zj} \right\} \tag{13,14}$$

where F_{xj}, F_{yj}, F_{zj} are the complex external forces in the x, y and z directions and T_{xj}, T_{yj}, T_{zj} are the complex external moments referred respectively to the x, y and z axis acting at position P_j of the source or receiver structures respectively.

The flanking excitation acting on the receiver $\mathbf{q}_f$ could be due to a subsystem connected with it or to a flanking path connecting the source with the receiver. The dynamics of the mounting system are expressed using an impedance matrix approach:

$$\mathbf{f}_m = \mathbf{Z}_m\mathbf{v}_m + \mathbf{V}_m\mathbf{q}_s \tag{15}$$

where $\mathbf{Z}_m$ is the impedance matrix of the mounting system which relates the linear and angular velocities at each end of the mounts to the forces and moments at each end of the mounts as well. $\mathbf{V}_m$ is the excitation matrix which gives the forces and moments at each end of the mounts due to the control excitations terms which are grouped in the $\mathbf{q}_s$ vector:

$$\mathbf{q}_s^T = \left\{ \mathbf{q}_{s1}^T \quad \mathbf{q}_{s2}^T \quad \cdots \quad \mathbf{q}_{sn}^T \right\} \tag{16}$$

where:

$$\mathbf{q}_{sj}^T = \left\{ F_{sxj} \quad F_{syj} \quad F_{szj} \quad T_{sxj} \quad T_{syj} \quad T_{szj} \right\} \tag{17}$$

and F_{sxj}, F_{syj}, F_{szj} are the complex control forces in x, y and z direction while T_{sxj}, T_{syj}, T_{szj} are the complex control torques with reference to the x, y and z axis applied at the P_j mount position. The source and receiver equations (9), (10) can be grouped together in one equation:

$$\mathbf{v}_{sr} = \mathbf{M}_{sr1}\mathbf{f}_{sr} + \mathbf{M}_{sr2}\mathbf{q}_{pf} \tag{18}$$

where the mobility matrices and the excitation vector have the form:

$$\mathbf{M}_{sr1} = \begin{bmatrix} \mathbf{M}_{s1} & \mathbf{0} \\ \mathbf{0} & \mathbf{M}_{r1} \end{bmatrix} \qquad \mathbf{M}_{sr2} = \begin{bmatrix} \mathbf{M}_{s2} & \mathbf{0} \\ \mathbf{0} & \mathbf{M}_{r2} \end{bmatrix} \qquad \mathbf{q}_{pf} = \begin{Bmatrix} \mathbf{q}_p \\ \mathbf{q}_f \end{Bmatrix} \tag{19-21}$$

and the junctions *velocity* and *force vectors* are given by:

$$\mathbf{v}_{sr} \equiv \begin{Bmatrix} \mathbf{v}_s \\ \mathbf{v}_r \end{Bmatrix} \qquad \mathbf{f}_{sr} \equiv \begin{Bmatrix} \mathbf{f}_s \\ \mathbf{f}_r \end{Bmatrix} \tag{22,23}$$

where $\mathbf{v}_{sr}$ and $\mathbf{f}_{sr}$ are called respectively source-receiver *velocity vector* and source-receiver *force vector*. The source receiver vectors are related to the analogous mounting system vectors by a *transformation matrix* $\mathbf{T}$ in such a way as to satisfy the compatibility condition (for the velocity vectors) and the equilibrium principle (for the force vectors) at each junction:

$$\mathbf{v}_m = \mathbf{T}\mathbf{v}_{sr} \qquad \mathbf{f}_m + \mathbf{T}\mathbf{f}_{sr} = 0 \tag{24,25}$$

Using these two relations, equations (18) and (15) can be related in such a way as to find the source-receiver velocity vector or the source-receiver force vector as a function of the primary-flanking and secondary excitation vectors:

$$\mathbf{v}_{sr} = \mathbf{Q}_{pv}\mathbf{q}_{pf} + \mathbf{Q}_{sv}\mathbf{q}_s \qquad \mathbf{f}_{sr} = \mathbf{Q}_{pf}\mathbf{q}_{pf} + \mathbf{Q}_{sf}\mathbf{q}_s \tag{26,27}$$

where: $$\mathbf{Q}_{pv} = \left(\mathbf{I} + \mathbf{M}_{sr1}\mathbf{T}^{-1}\mathbf{Z}_{m1}\mathbf{T}\right)^{-1}\mathbf{M}_{sr2} \tag{28}$$

$$\mathbf{Q}_{sv} = -\left(\mathbf{I} + \mathbf{M}_{sr1}\mathbf{T}^{-1}\mathbf{Z}_{m1}\mathbf{T}\right)^{-1}\mathbf{M}_{sr1}\mathbf{T}^{-1}\mathbf{Z}_{m2} \tag{29}$$

$$\mathbf{Q}_{pf} = -\mathbf{T}^{-1}\mathbf{Z}_{m1}\mathbf{T}\left(\mathbf{I} + \mathbf{M}_{sr1}\mathbf{T}^{-1}\mathbf{Z}_{m1}\mathbf{T}\right)^{-1}\mathbf{M}_{sr2} \tag{30}$$

$$\mathbf{Q}_{sf} = \mathbf{T}^{-1}\mathbf{Z}_{m1}\mathbf{T}\left(\mathbf{I} + \mathbf{M}_{sr1}\mathbf{T}^{-1}\mathbf{Z}_{m1}\mathbf{T}\right)^{-1}\mathbf{M}_{sr1}\mathbf{T}^{-1}\mathbf{Z}_{m2} - \mathbf{T}^{-1}\mathbf{Z}_{m2} \tag{31}$$

With this model the vibration transmission at each junction is characterised by both kinematic (linear and angular velocities) and dynamic (forces and moments) parameters such that two types of problem arise: first, it is impossible to directly compare the vibration transmission associated with angular velocity and linear velocity or associated with moment and force and second, the standard approach of using either only velocities or only forces to represent the system's vibrations does not give sufficient information about the effective vibration transmission. Goyder and White [19] have suggested that these two problems can be overcome in the case of isolation of vibration transmission from a rigid source to a flexible receiver by representing the vibration transmission in terms of total structural power transmitted to the receiver. This single parameter accounts for the vibration contribution of **all 6 kinematic** and **6 dynamic** parameters at the junctions between the source and receiver structure. This approach has been used in other studies as can be seen from references [20-25]. The model used in this study allows this approach to be extended to a multiple mount and multiple degrees-of-freedom complete isolation system [26]. In fact, using equations (24) and (25) it is possible to express the *time-averaged total power* transmitted to the receiver system in terms of the primary vector and the control vector by using the following equation

$$P = 1/2\,\mathrm{Re}\left\{\mathbf{f}_r^H \mathbf{v}_r\right\} \tag{32}$$

where $\mathbf{f}_r$ and $\mathbf{v}_r$ represent respectively the force and velocity at the receiver structure.

Because the ultimate aim of the study carried out is related to isolation of structure-borne noise transmission it has been preferred to represent the vibration of the receiver structure in terms of its kinetic energy associated only to the bending wave motion which originates the sound radiation. The kinetic energy related to the bending motion of a thin bi-dimensional structure is given by the following relation:

$$K = \int_S \rho h \left|\dot{w}(s,t)\right|^2 dS \tag{33}$$

where ρ is the density of the material, S is the area of the structure and $h(s,t)$, $\dot{w}(s,t)$ are respectively the thickness and the out-of-plane velocity at position (s,t) of the structure.

3. CONTROL STRATEGIES

All of the active control strategies considered in the study here summarised can be expressed in terms of a quadratic cost function which is minimised and this can always be written in the form [27]:

$$J = \mathbf{q}_s^H \mathbf{A} \mathbf{q}_s + \mathbf{q}_s^H \mathbf{b} + \mathbf{b}^H \mathbf{q}_s + c \ . \tag{34}$$

The control source that minimises this quadratic equation is given by [27]:

$$\mathbf{q}_{s0} = -\mathbf{A}^{-1}\mathbf{b} \tag{35}$$

The control strategy of (i) *minimising total power transmitted by the source to the receiver* was assumed as a reference for assessing the efficacy of the cost function studied which are the (ii) *cancellation of out-of-plane input velocities to the receiver* and the (iii) *cancellation of out-of-plane input forces to the receiver.* In this report these three control strategies will be referred to as: (i) *total power* minimisation (J_p), (ii) *velocity* cancellation (J_v) and (iii) *force* cancellation (J_f). When the total power is minimised the cost function is:

$$J_p = \frac{1}{2}\mathrm{Re}\left(\mathbf{f}_r^H \mathbf{v}_r\right) = \frac{1}{4}\left(\mathbf{f}_r^H \mathbf{v}_r + \mathbf{v}_r^H \mathbf{f}_r\right) \tag{36}$$

where the receiver velocities and forces parameters at the receiver junctions are given by the two following equations $\mathbf{v}_r = \mathbf{R}_{r1}\mathbf{v}_{sr}$ and $\mathbf{f}_r = \mathbf{R}_{r1}\mathbf{f}_{sr}$ where $\mathbf{R}_{r1} = \left[\mathbf{0}_{t\times t} \quad \mathbf{I}_{t\times t}\right]$ and $\mathbf{0}_{t\times t}$, $\mathbf{I}_{t\times t}$ are respectively a zero matrix and a unit matrix, t is the dimension of the source and receiver vectors. The two matrices in the quadratic form of equation (33) are then needed

$$\mathbf{A}_p = \frac{1}{4}\left(\mathbf{Q}_{sf}^H \mathbf{R}_{r1}^T \mathbf{R}_{r1} \mathbf{Q}_{sv} + \mathbf{Q}_{sv}^H \mathbf{R}_{r1}^T \mathbf{R}_{r1} \mathbf{Q}_{sf}\right) \qquad \mathbf{b}_p = \frac{1}{4}\left(\mathbf{Q}_{sf}^H \mathbf{R}_{r1}^T \mathbf{R}_{r1} \mathbf{Q}_{pv} \mathbf{q}_{pf} + \mathbf{Q}_{sv}^H \mathbf{R}_{r1}^T \mathbf{R}_{r1} \mathbf{Q}_{pf} \mathbf{q}_{pf}\right) \tag{37,38}$$

When velocity cancellation is implemented then the cost function has the form:

$$J_v = \mathbf{v}_r^H \mathbf{v}_r \tag{39}$$

and the velocity vector $\mathbf{v}_r$ is obtained with the following equation $\mathbf{v}_r = \mathbf{R}_{r2}\mathbf{v}_{sr}$ with $\mathbf{R}_{r1} = \left[\mathbf{0}_{t\times t} \quad \mathbf{H}_{t\times t}\right]$ and $\mathbf{H}_{t\times t}$ is a zero matrix with diagonal unit terms in correspondence of the row/column related to the z axis . The two matrices in equation (33) are then given by:

$$\mathbf{A}_v = \mathbf{Q}_{sv}^H \mathbf{R}_{r2}^T \mathbf{R}_{r2} \mathbf{Q}_{sv} \qquad \mathbf{b}_v = \mathbf{Q}_{sv}^H \mathbf{R}_{r2}^T \mathbf{R}_{r2} \mathbf{Q}_{pv} \mathbf{q}_{pf} \tag{40, 41}$$

When force cancellation is implemented then the cost function has the form:

$$J_f = \mathbf{f}_r^H \mathbf{f}_r \tag{42}$$

and the force vector $\mathbf{f}_r$ is obtained with the following equation $\mathbf{f}_r = \mathbf{R}_{r2}\mathbf{f}_{sr}$. The two matrices in equation (33) are then given by:

$$\mathbf{A}_f = \mathbf{Q}_{sf}^H \mathbf{R}_{r2}^T \mathbf{R}_{r2} \mathbf{Q}_{sf} \qquad \mathbf{b}_f = \mathbf{Q}_{sf}^H \mathbf{R}_{r2}^T \mathbf{R}_{r2} \mathbf{Q}_{pf} \mathbf{q}_{pf} \tag{43, 44}$$

4. THE SYSTEMS STUDIED

Figure 2 shows the geometry of the system studied. The source and receiver structures are freely suspended aluminium plates having dimensions $l_{xs} \times l_{ys} = l_{xr} \times l_{yr} = 1.2 \times 1.0$ m and thickness $t_s = 3$ mm, $t_r = 1.5$ mm. The physical properties of the two plates are: density $\rho_s = \rho_r = 2796$ Kg/m^3, Young's modulus of elasticity $E_s = E_r = 7.24 \times 10^{10}$ N/m^2, Poisson ratio $\nu_s = \nu_r = 0.3$, loss factor $\eta_s = \eta_r = 0.01$. The three mounts are modelled as cylinders of soft rubber with either a single inertial control force acting at the top end of the mounts or two reactive control forces acting at both mount's ends. The diameter and the height of the suspensions are respectively $\phi_m = 15$ mm and $h_m = 15$ mm while the physical properties of the rubber are: density $\rho_m = 1078$ Kg/m^3, Young's modulus of elasticity $E_m = 1.5 \times 10^6$ N/m^2, Poisson ratio $\nu_m = 0.49$ and loss factor $\eta_m = 0.05$. Also, a stiffer mounting system has been modelled by assuming the mounts as cylinders of aluminium with physical properties: $\rho_m = 2796$ Kg/m^3, $E_m = 7.24 \times 10^{10}$ N/m^2, $\nu_m = 0.3$ $\eta_m = 0.01$. The effects generated by the components used to connect the mounting system to the plates and to connect force and velocity sensors at the top of the mounts has been modelled as a pair of rectangular parallelepiped block masses connected at the mounts ends. The dimensions and weight of the masses attached to the top side of the mounts are: $d_{xt} \times d_{yt} \times d_{zt} = 12 \times 12 \times 24$ mm, $W_t = 9.8 \times 10^{-3}$ Kg while the dimensions and weight of the masses attached to the bottom side of the mounts are: $d_{xb} \times d_{yb} \times d_{zb} = 8 \times 8 \times 8$ mm, $W_b = 3.1 \times 10^{-3}$ Kg.

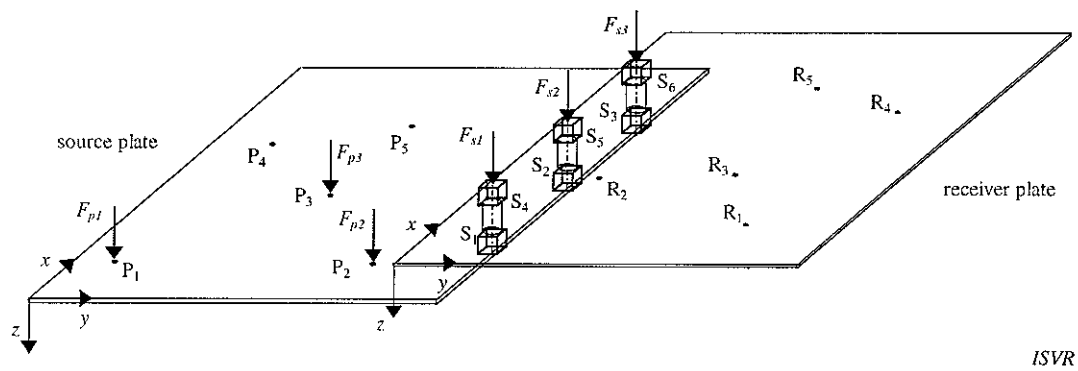

Figure 2: The system studied.

The source and receiver thin plates are assumed to be distributed elements and the model considers only the effect of bending waves. In-plane shear and longitudinal waves are neglected since their sound radiation effect is negligible and their coupling to the bending motion of the plate themselves due to the mounting system is also negligible. The mounts are modelled as distributed systems on which longitudinal and flexural waves can propagate.

Therefore the matrix model described in section 2 has been used by considering only three degrees of freedom at the mounts junctions and at the excitation positions. The velocity and force junction vectors of equations (1,2) have therefore been assumed as follow:

$$\mathbf{v}_j^T \equiv \left\{ \dot{w}_j \quad \dot{\theta}_{xj} \quad \dot{\theta}_{yj} \right\} \qquad \mathbf{f}_j^T \equiv \left\{ N_{zj} \quad M_{xj} \quad M_{yj} \right\} \tag{45,46}$$

where $\dot{w}_j$ is the linear velocity in the z direction, $\dot{\theta}_{xj}$ and $\dot{\theta}_{yj}$ are the angular velocities referred respectively to the x and y axis, N_{zj} is the force in the z direction and M_{xj}, M_{yj} are the moments referred respectively to the x and y axis. The positions of the mounts junctions at the source (S_1, S_2, S_3) and receiver (S_4, S_5, S_6) plates are given in tables 1 and 2.

Tab 1: mounts junction positions' at the source plate

	x (m)	y (m)
S_1	0.2	0.991
S_2	0.6	0.991
S_3	1	0.991

Tab 2: mounts junction positions' at the receiver plate

	x (m)	y (m)
S_4	0.2	0.009
S_5	0.6	0.009
S_6	1	0.009

Three primary excitation positions have been selected in such a way to coincide with the first three monitoring positions P_1, P_2, P_3 of the source plate. The jth excitation vector is composed by three components: an out-of-plane force in z direction F_{zj} and two torques in x and y directions T_{xj} and T_{yj} so that:

$$\mathbf{q}_{pj}^T \equiv \left\{ F_{zj} \quad T_{xj} \quad T_{yj} \right\} \tag{47}$$

Finally, because only inertial or reactive axial control actuators has been considered the control vector $\mathbf{q}_{sj}$ of equation (17) assumes the following form:

$$\mathbf{q}_{sj}^T \equiv F_{szj} \tag{48}$$

The monitoring positions of the source P_1, P_2, ..., P_5 and receiver R_1, R_2, ..., R_5 plates are summarised in tables 3 and 4.

Tab 3: monitoring positions at the source plate

	x (m)	y (m)
P_1	0.26	0.175
P_2	0.26	0.82
P_3	0.55	0.475
P_4	0.77	0.195
P_5	0.96	0.43

Tab 4: monitoring positions at the receiver plate

	x (m)	y (m)
R_1	0.26	0.64
R_2	0.42	0.18
R_3	0.55	0.525
R_4	0.77	0.805
R_5	0.96	0.57

These positions are called monitoring positions since, for practical purposes, they have been chosen to represent the vibrations level of the source and receiver plates by an estimate of the plates kinetic energy associated to the bending motion which is given by the sum of the squared values of the out-of-plane velocities at the plates' monitoring positions exactly!:

$$K_{Es} = \mathbf{v}_P^H \mathbf{v}_P \qquad K_{Er} = \mathbf{v}_R^H \mathbf{v}_R \tag{49,50}$$

where:

$$\mathbf{v}_P^T = \{\dot{w}_{P1} \quad \dot{w}_{P2} \quad \dot{w}_{P3} \quad \dot{w}_{P4} \quad \dot{w}_{P5}\} \qquad \mathbf{v}_R^T = \{\dot{w}_{R1} \quad \dot{w}_{R2} \quad \dot{w}_{R3} \quad \dot{w}_{R4} \quad \dot{w}_{R5}\} \tag{51,52}$$

The estimate of the source and receiver kinetic energy has been used to compare and validate the matrix model used in this study with experimental measurements taken on a similar system.

No flanking excitation was considered acting on the receiver plate so that the matrix equations (9) and (10) assume respectively the following forms:

$$\begin{Bmatrix} \mathbf{v}_{S1} \\ \mathbf{v}_{S2} \\ \mathbf{v}_{S3} \end{Bmatrix} = \begin{bmatrix} \mathbf{M}_{S1S1} & \mathbf{M}_{S1S2} & \mathbf{M}_{S1S3} \\ \mathbf{M}_{S2S1} & \mathbf{M}_{S2S2} & \mathbf{M}_{S2S3} \\ \mathbf{M}_{S3S1} & \mathbf{M}_{S3S2} & \mathbf{M}_{S3S3} \end{bmatrix} \begin{Bmatrix} \mathbf{f}_{S1} \\ \mathbf{f}_{S2} \\ \mathbf{f}_{S3} \end{Bmatrix} + \begin{bmatrix} \mathbf{M}_{S1P1} & \mathbf{M}_{S1P2} & \mathbf{M}_{S1P3} \\ \mathbf{M}_{S2P1} & \mathbf{M}_{S2P2} & \mathbf{M}_{S2P3} \\ \mathbf{M}_{S3P1} & \mathbf{M}_{S3P2} & \mathbf{M}_{S3P3} \end{bmatrix} \begin{Bmatrix} \mathbf{q}_{P1} \\ \mathbf{q}_{P2} \\ \mathbf{q}_{P3} \end{Bmatrix} \tag{53}$$

$$\begin{Bmatrix} \mathbf{v}_{S4} \\ \mathbf{v}_{S5} \\ \mathbf{v}_{S6} \end{Bmatrix} = \begin{bmatrix} \mathbf{M}_{S4S4} & \mathbf{M}_{S4S5} & \mathbf{M}_{S4S6} \\ \mathbf{M}_{S5S4} & \mathbf{M}_{S5S5} & \mathbf{M}_{S5S6} \\ \mathbf{M}_{S6S4} & \mathbf{M}_{S6S5} & \mathbf{M}_{S6S6} \end{bmatrix} \begin{Bmatrix} \mathbf{f}_{S4} \\ \mathbf{f}_{S5} \\ \mathbf{f}_{S6} \end{Bmatrix}. \tag{54}$$

Because the mounts are all equal the impedance equation (15) assumes a simplified form which is given by the following two equations in the case of a reactive or an inertial control force scheme respectively:

$$\begin{Bmatrix} \mathbf{f}_{S1} \\ \mathbf{f}_{S2} \\ \mathbf{f}_{S3} \\ \mathbf{f}_{S4} \\ \mathbf{f}_{S5} \\ \mathbf{f}_{S6} \end{Bmatrix} = \begin{bmatrix} \mathbf{Z}_{11} & \mathbf{0} & \mathbf{0} & \mathbf{Z}_{12} & \mathbf{0} & \mathbf{0} \\ \mathbf{0} & \mathbf{Z}_{11} & \mathbf{0} & \mathbf{0} & \mathbf{Z}_{12} & \mathbf{0} \\ \mathbf{0} & \mathbf{0} & \mathbf{Z}_{11} & \mathbf{0} & \mathbf{0} & \mathbf{Z}_{12} \\ \mathbf{Z}_{21} & \mathbf{0} & \mathbf{0} & \mathbf{Z}_{22} & \mathbf{0} & \mathbf{0} \\ \mathbf{0} & \mathbf{Z}_{21} & \mathbf{0} & \mathbf{0} & \mathbf{Z}_{22} & \mathbf{0} \\ \mathbf{0} & \mathbf{0} & \mathbf{Z}_{21} & \mathbf{0} & \mathbf{0} & \mathbf{Z}_{22} \end{bmatrix} \begin{Bmatrix} \mathbf{v}_{S1} \\ \mathbf{v}_{S2} \\ \mathbf{v}_{S3} \\ \mathbf{v}_{S4} \\ \mathbf{v}_{S5} \\ \mathbf{v}_{S6} \end{Bmatrix} + \begin{bmatrix} -\mathbf{V}_1 & \mathbf{0} & \mathbf{0} \\ \mathbf{0} & -\mathbf{V}_1 & \mathbf{0} \\ \mathbf{0} & \mathbf{0} & -\mathbf{V}_1 \\ \mathbf{V}_1 & \mathbf{0} & \mathbf{0} \\ \mathbf{0} & \mathbf{V}_1 & \mathbf{0} \\ \mathbf{0} & \mathbf{0} & \mathbf{V}_1 \end{bmatrix} \begin{Bmatrix} \mathbf{q}_{s1} \\ \mathbf{q}_{s2} \\ \mathbf{q}_{s3} \end{Bmatrix}; \tag{55}$$

$$\begin{Bmatrix} \mathbf{f}_{S1} \\ \mathbf{f}_{S2} \\ \mathbf{f}_{S3} \\ \mathbf{f}_{S4} \\ \mathbf{f}_{S5} \\ \mathbf{f}_{S6} \end{Bmatrix} = \begin{bmatrix} \mathbf{Z}_{11} & \mathbf{0} & \mathbf{0} & \mathbf{Z}_{12} & \mathbf{0} & \mathbf{0} \\ \mathbf{0} & \mathbf{Z}_{11} & \mathbf{0} & \mathbf{0} & \mathbf{Z}_{12} & \mathbf{0} \\ \mathbf{0} & \mathbf{0} & \mathbf{Z}_{11} & \mathbf{0} & \mathbf{0} & \mathbf{Z}_{12} \\ \mathbf{Z}_{21} & \mathbf{0} & \mathbf{0} & \mathbf{Z}_{22} & \mathbf{0} & \mathbf{0} \\ \mathbf{0} & \mathbf{Z}_{21} & \mathbf{0} & \mathbf{0} & \mathbf{Z}_{22} & \mathbf{0} \\ \mathbf{0} & \mathbf{0} & \mathbf{Z}_{21} & \mathbf{0} & \mathbf{0} & \mathbf{Z}_{22} \end{bmatrix} \begin{Bmatrix} \mathbf{v}_{S1} \\ \mathbf{v}_{S2} \\ \mathbf{v}_{S3} \\ \mathbf{v}_{S4} \\ \mathbf{v}_{S5} \\ \mathbf{v}_{S6} \end{Bmatrix} + \begin{bmatrix} \mathbf{0} & \mathbf{0} & \mathbf{0} \\ \mathbf{0} & \mathbf{0} & \mathbf{0} \\ \mathbf{0} & \mathbf{0} & \mathbf{0} \\ \mathbf{V}_1 & \mathbf{0} & \mathbf{0} \\ \mathbf{0} & \mathbf{V}_1 & \mathbf{0} \\ \mathbf{0} & \mathbf{0} & \mathbf{V}_1 \end{bmatrix} \begin{Bmatrix} \mathbf{q}_{s1} \\ \mathbf{q}_{s2} \\ \mathbf{q}_{s3} \end{Bmatrix}. \tag{56}$$

Expressions for the mobility $\mathbf{M}_{ij}$, impedance $\mathbf{Z}_{ij}$ and excitation matrix $\mathbf{V}_1$ matrices are given in appendices A and B.

Once the force parameters at the mounting junction positions are calculated with equation (27) it is possible to derive the out of plane velocities at the monitoring positions of the source and receiver plate with the following two relations:

$$\begin{Bmatrix} \dot{w}_{P1} \\ \dot{w}_{P2} \\ \dot{w}_{P3} \\ \dot{w}_{P4} \\ \dot{w}_{P5} \end{Bmatrix} = \begin{bmatrix} \mathbf{M}_{P1S1} & \mathbf{M}_{P1S2} & \mathbf{M}_{P1S3} \\ \mathbf{M}_{P2S1} & \mathbf{M}_{P2S2} & \mathbf{M}_{P2S3} \\ \mathbf{M}_{P3S1} & \mathbf{M}_{P3S2} & \mathbf{M}_{P3S3} \\ \mathbf{M}_{P4S1} & \mathbf{M}_{P4S2} & \mathbf{M}_{P4S3} \\ \mathbf{M}_{P5S1} & \mathbf{M}_{P5S2} & \mathbf{M}_{P5S3} \end{bmatrix} \begin{Bmatrix} \mathbf{f}_{S1} \\ \mathbf{f}_{S2} \\ \mathbf{f}_{S3} \end{Bmatrix} \qquad \begin{Bmatrix} \dot{w}_{R1} \\ \dot{w}_{R2} \\ \dot{w}_{R3} \\ \dot{w}_{R4} \\ \dot{w}_{R5} \end{Bmatrix} = \begin{bmatrix} \mathbf{M}_{R1S4} & \mathbf{M}_{R1S5} & \mathbf{M}_{R1S6} \\ \mathbf{M}_{R2S4} & \mathbf{M}_{R2S5} & \mathbf{M}_{R2S6} \\ \mathbf{M}_{R3S4} & \mathbf{M}_{R3S5} & \mathbf{M}_{R3S6} \\ \mathbf{M}_{R4S4} & \mathbf{M}_{R4S5} & \mathbf{M}_{R4S6} \\ \mathbf{M}_{R5S4} & \mathbf{M}_{R5S5} & \mathbf{M}_{R5S6} \end{bmatrix} \begin{Bmatrix} \mathbf{f}_{S4} \\ \mathbf{f}_{S5} \\ \mathbf{f}_{S6} \end{Bmatrix} \tag{57,58}$$

5. VIBRATION TRANSMISSION WITH PASSIVE AND ACTIVE ISOLATORS

5.1 Plates connected by a single mount

The first set of results presented refer to a case where only one mount connects the two plates at positions S_2 and S_5.

The results shown at pages 14, 15 and 16 (figures 3 to 14) refer to three particular configurations of the mounting system:

case 1. rubber or aluminium mount with an inertial control actuator modelled as a sky hook force acting at the top end of the mount which has not lumped masses at the top and bottom ends;

case 2. rubber or aluminium mount with lumped masses at the top and bottom ends ($W_t = 9.8\times10^{-3}$ Kg $W_b = 3.1\times10^{-3}$ Kg) and with an inertial control actuator modelled as a sky hook force acting at the top end of the mount;

case 3. rubber or aluminium mount with lumped masses at the top and bottom ends ($W_t = 9.8\times10^{-3}$ Kg $W_b = 3.1\times10^{-3}$ Kg) and with a reactive control actuator modelled as pair of reactive forces acting at the bottom and top ends of the mount.

For each case two plots have been produced: the first (top plot) shows the estimate of kinetic energy at the source and receiver panels calculated with equations 49 and 50 when a harmonic unit primary force F_{P3} is exciting the system, while the second (bottom plot) shows the estimate of kinetic energy at the receiver panels when a harmonic unit primary force F_{P3} is exciting the system and the secondary forces are set in such a way to implement the power minimisation, velocity and force cancellation cost functions described in section 3. The two plots are shown for both the case of a rubber isolator (plots on the left side) and the case of an aluminium isolator (plots on the right side).

The picture that comes from this set of simulations can be summarised in the following points.

1. The passive isolation provided by the mount varies substantially depending on the type of material it is made of. Figure 3 shows that the rubber mount produces good isolation effects. At frequencies below 250 Hz the isolation is very little but as the frequency rises the isolation effect increases up to about 40 dB at 1 kHz. Figure 5 shows instead a much smaller isolation effect if the mount is made of aluminium; there is no isolation below 500 Hz and at about 1 kHz the structural vibration transmission is reduced to about 15 dB only.
2. When the two block masses are applied at the rubber mount ends an extra passive isolation effect is obtained which, by comparing figures 3 and 7, can be estimated to be about 10 dB at 1 kHz. When the aluminium isolator is used the presence of the block masses at each end of the mounts seems to be ineffective as can be deduced by comparing figures 5 and 9.
3. In general the three control strategies under study, power minimisation and force or velocity cancellation, have given similar control effects in the three cases examined.
4. Comparing the results of case 3 with those of case 2, no major differences have been detected when the reactive actuator is used in place of the inertial actuator.

5. The presence of block masses mounted at the isolator ends does not produce significant effects on the control performances.
6. The rubber active isolator gives very good control performance which, as shown by figures 4, 8 and 12, goes from a maximum of about 60 dB reduction at very low frequency to a minimum of about 10 dB at about 1 kHz.
7. The aluminium active isolator gives instead very poor control performances which are of the order of a few dB at very narrow frequency bands (for example between 250 and 300 Hz of figure 6) and can be considered negligible at the remaining frequencies.

A final case, case 4, is presented which considers the isolation effectiveness of the system with rubber or aluminium mounts with lumped masses at the top and bottom ends ($W_t = 9.8\times10^{-3}$ Kg $W_b = 3.1\times10^{-3}$ Kg) and with an inertial control actuator modelled as a sky hook force acting at the top end of the mount when the primary harmonic unit excitation is acting either at position P_1, P_2 and P_3 . Only the effectiveness of the velocity cancellation control strategy has been analysed.

Figure 15 shows that both the rubber and the aluminium isolator control capabilities are not affected by the position of the primary excitation.

CASE 1.

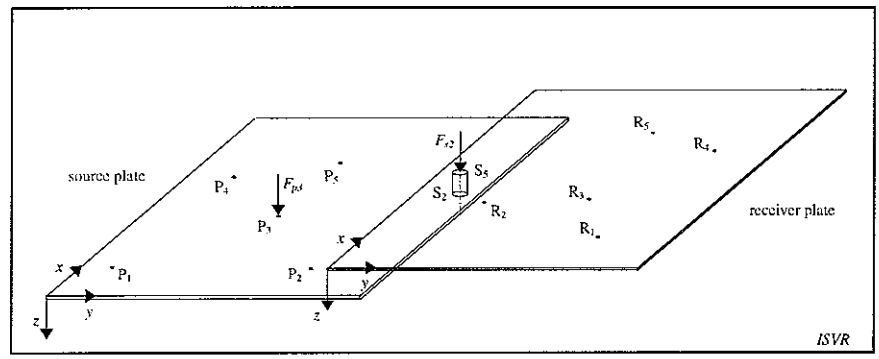

RUBBER

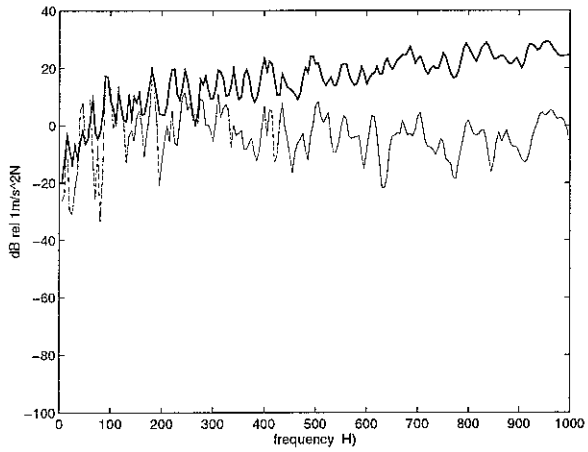

Figure 3: Estimate of the source K_{Es} (solid line) and receiver K_{Er} (faint) kinetic energy when the primary force F_{p3} is exciting the two panel system with one rubber mount without block masses and an inertial control force.

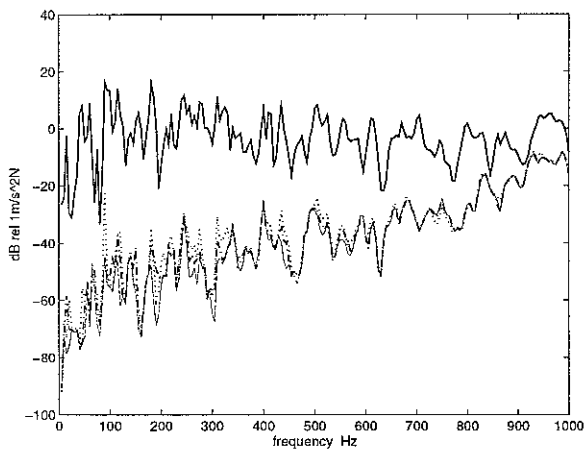

Figure 4: Estimate of the receiver K_{Er} kinetic energy when the primary force F_{p3} is exciting the two panel system with one rubber mount without block masses and an inertial control force. Solid line, without control; faint line, when total power is minimised; dotted line, when forces are cancelled; dash-dotted line when velocities are cancelled.

ALUMINIUM

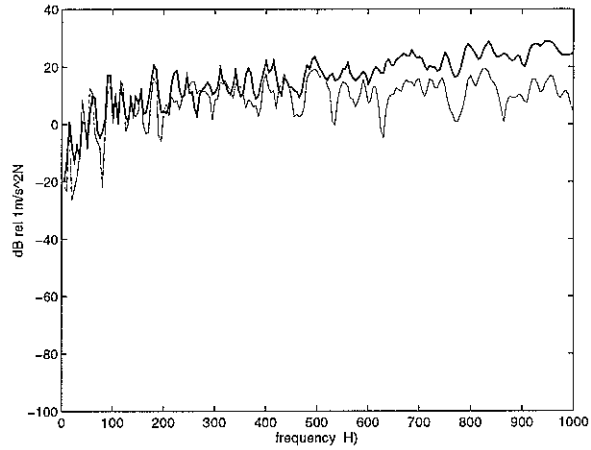

Figure 5: Estimate of the source K_{Es} (solid line) and receiver K_{Er} (faint) kinetic energy when the primary force F_{p3} is exciting the two panel system with one aluminium mount without block masses and an inertial control force.

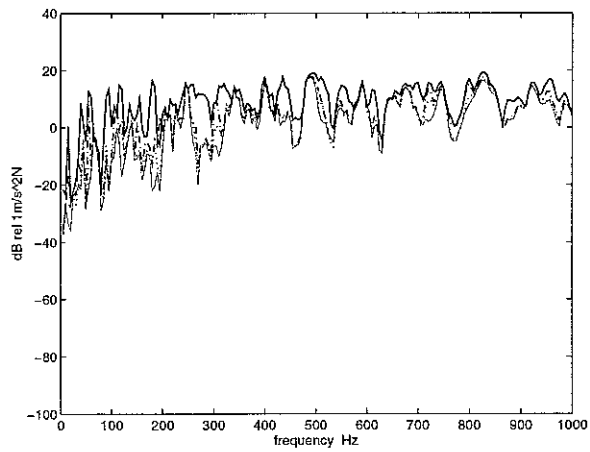

Figure 6: Estimate of the receiver K_{Er} kinetic energy when the primary force F_{p3} is exciting the two panel system with one aluminium mount without block masses and an inertial control force. Solid line, without control; faint line, when total power is minimised; dotted line, when forces are cancelled; dash-dotted line when velocities are cancelled.

CASE 2.

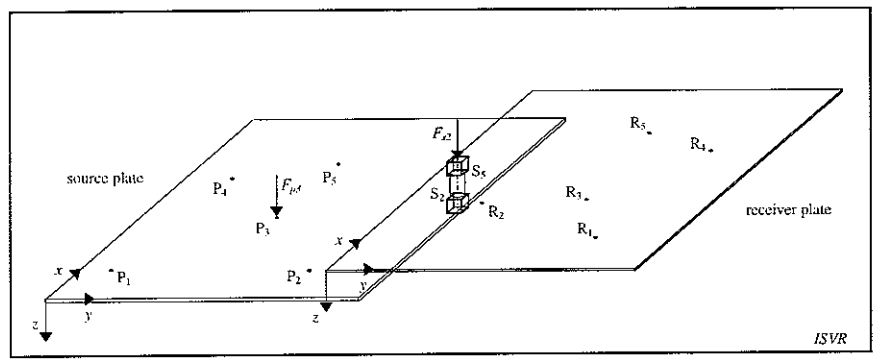

RUBBER

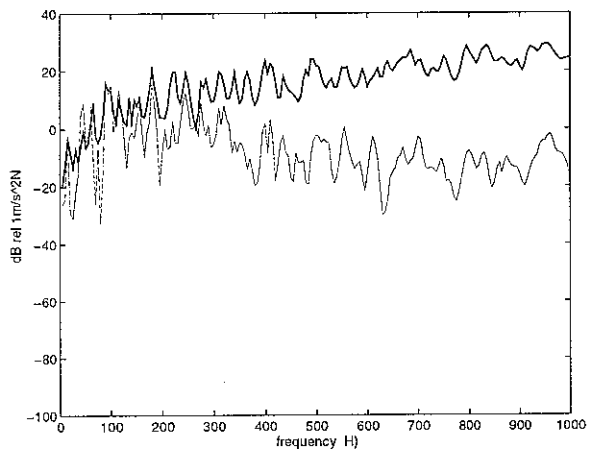

Figure 7: Estimate of the source K_{Es} (solid line) and receiver K_{Er} (faint) kinetic energy when the primary force F_{p3} is exciting the two panel system with one rubber mount with block masses and an inertial control force.

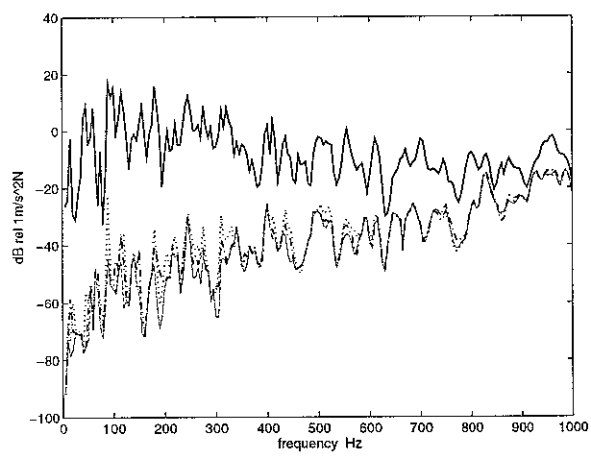

Figure 8: Estimate of the receiver K_{Er} kinetic energy when the primary force F_{p3} is exciting the two panel system with one rubber mount with block masses and an inertial control force. Solid line, without control; faint line, when total power is minimised; dotted line, when forces are cancelled; dash-dotted line when velocities are cancelled.

ALUMINIUM

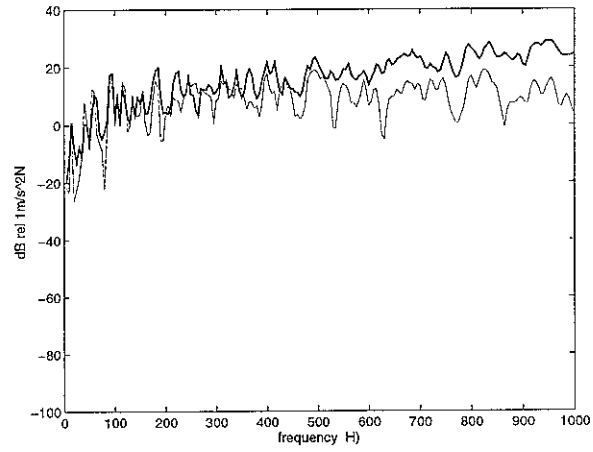

Figure 9: Estimate of the source K_{Es} (solid line) and receiver K_{Er} (faint) kinetic energy when the primary force F_{p3} is exciting the two panel system with one aluminium mount with block masses and an inertial control force.

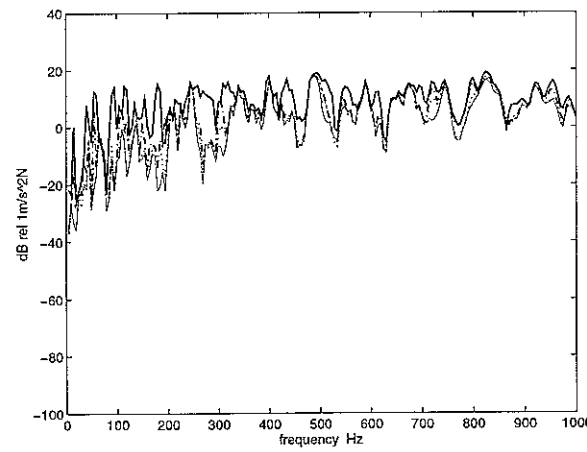

Figure 10: Estimate of the receiver K_{Er} kinetic energy when the primary force F_{p3} is exciting the two panel system with one aluminium mount with block masses and an inertial control force. Solid line, without control; faint line, when total power is minimised; dotted line, when forces are cancelled; dash-dotted line when velocities are cancelled.

CASE 3.

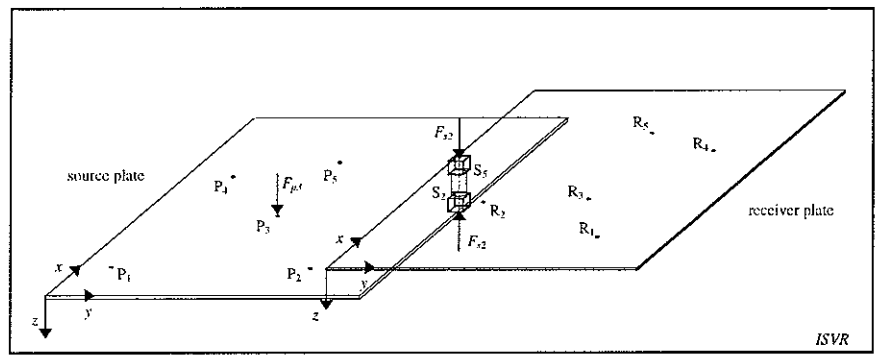

RUBBER

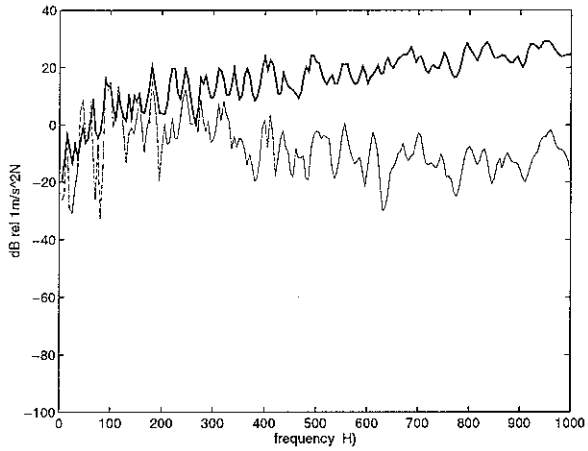

Figure 11: Estimate of the source K_{Es} (solid line) and receiver K_{Er} (faint) kinetic energy when the primary force F_{p3} is exciting the two panel system with one rubber mount with block masses and a pair of reactive control forces.

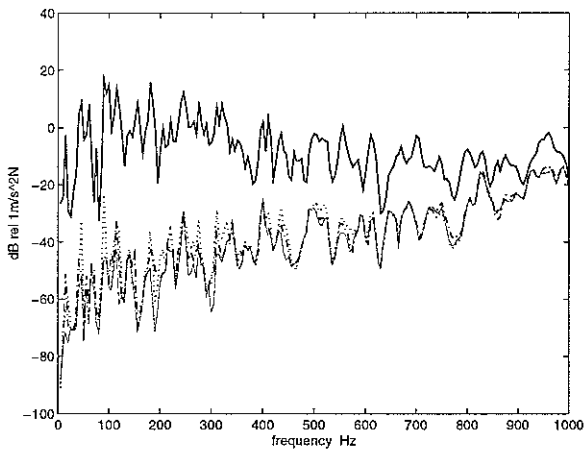

Figure 12: Estimate of the receiver K_{Er} kinetic energy when the primary force F_{p3} is exciting the two panels system with one rubber mount with block masses and a pair of reactive control forces. Solid line, without control; faint line, when total power is minimised; dotted line, when forces are cancelled; dash-dotted line when velocities are cancelled.

ALUMINIUM

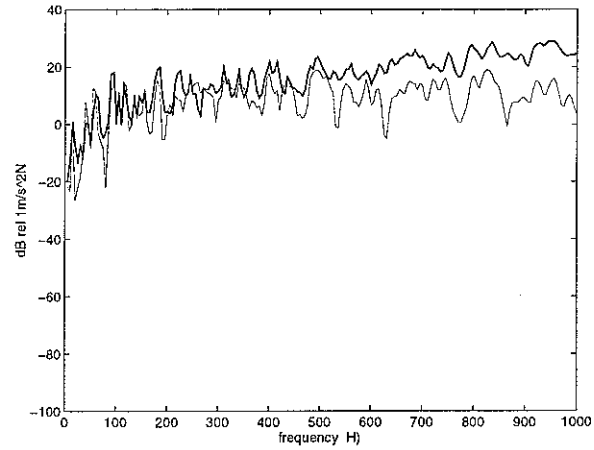

Figure 13: Estimate of the source K_{Es} (solid line) and receiver K_{Er} (faint) kinetic energy when the primary force F_{p3} is exciting the two panel system with one aluminium mount with block masses and a pair of reactive control forces.

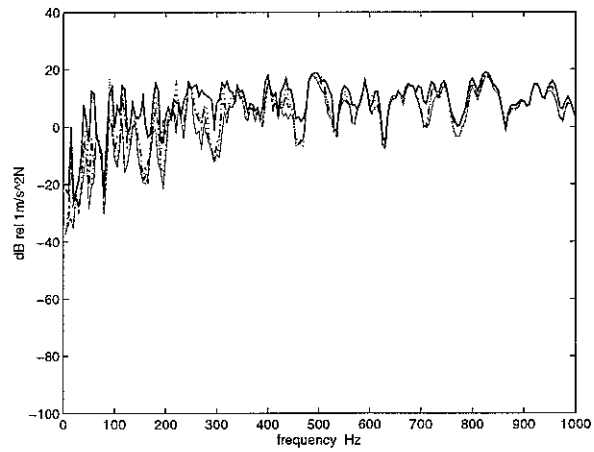

Figure 14: Estimate of the receiver K_{Er} kinetic energy when the primary force F_{p3} is exciting the two panel system with one aluminium mount with block masses and a pair of reactive control forces. Solid line, without control; faint line, when total power is minimised; dotted line, when forces are cancelled; dash-dotted line when velocities are cancelled.

CASE 4.

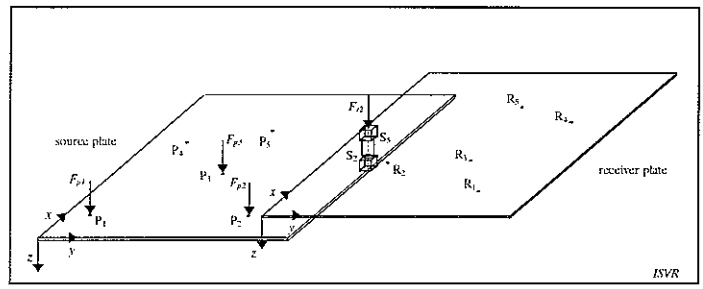

RUBBER **ALUMINIUM**

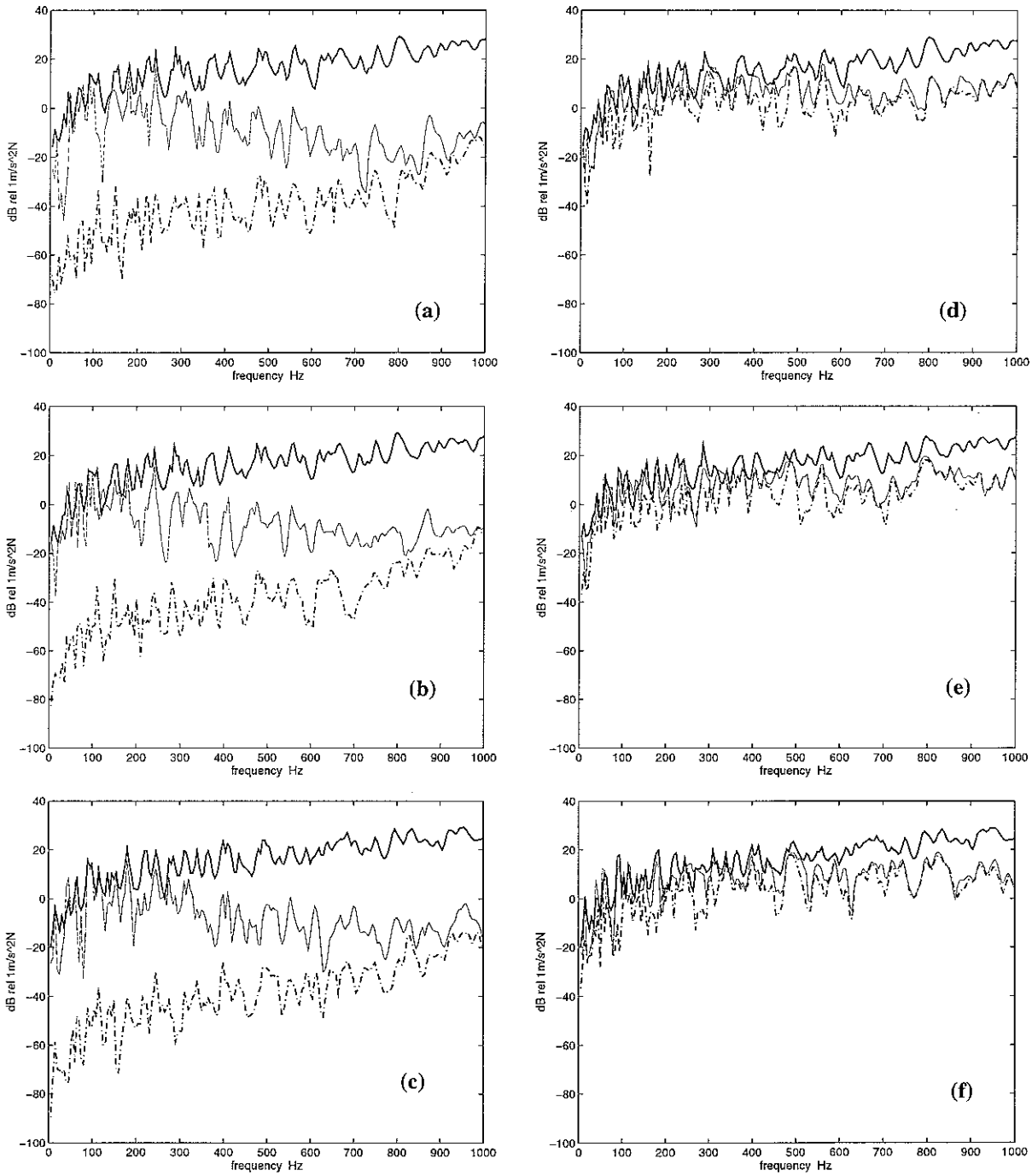

Figure 15: Estimate of the source K_{Es} kinetic energy (solid line) and receiver K_{Er} kinetic energy without (faint line) and with (dash-dotted line) active control when the primary force (a,d) F_{p1} (b,e) F_{p2} (c,f) F_{p3} is exciting the two panel system with either one rubber (cases a,b,c) or one aluminium (cases d,e,f) mount with block masses and an inertial control force.

5.2 Plates connected by three mounts

The second set of results presented refer to a case where three mounts connect the two plates as shown in the sketch of figure 2.

The results shown on pages 20, 21 and 22 (figures 16 to 28) refer to the three configurations of the mounting system considered in the previous section which are now grouped in the following cases:

case 5. rubber or aluminium mounts with inertial control actuators modelled as sky hook forces acting at the top end of the mounts which have no lumped masses at the top and bottom ends;

case 6. rubber or aluminium mounts with lumped masses at the top and bottom ends ($W_t = 9.8\times10^{-3}$ Kg $W_b = 3.1\times10^{-3}$ Kg) and with inertial control actuators modelled as sky hook forces acting at the top end of the mounts;

case 7. rubber or aluminium mounts with lumped masses at the top and bottom ends ($W_t = 9.8\times10^{-3}$ Kg $W_b = 3.1\times10^{-3}$ Kg) and with reactive control actuators modelled as a pair of reactive forces acting at the bottom and top ends of the mounts.

In a consistent way to the result exposition of previous section, for each case two plots have been produced: the first (top plot) shows the estimate of kinetic energy at the source and receiver panels calculated with equations 49 and 50, when a harmonic unit primary force F_{P3} is exciting the system, while the second (bottom plot) shows the estimate of kinetic energy at the receiver panels when a harmonic unit primary force F_{P3} is exciting the system, and the secondary forces are set in such a way to implement the power minimisation, velocity and force cancellation cost functions described in section 3. The two plots are shown for both the case of a rubber isolator (plots on the left side) and the case of an aluminium isolator (plots on the right side).

The analysis of these three cases can be summarised in the following points.

1. As found for the single mount isolator the isolator with three rubber mounts provides better passive isolation effects than that with three aluminium mounts. Considering figure 16, it can be seen that the rubber mounts produce good isolation effects above 300 Hz which could reach a level of about 30 dB at 1 kHz. However, the use of multiple mount does not increase the control performance, on the contrary it degrades the isolation potentiality of the single mount as can be seen by comparing figures 3 and 16.

   The aluminium mounting system gives a much smaller isolation effect than the rubber mounting system. Figure 18 shows that there is no isolation below 600 Hz and at about 1 kHz the structural vibration transmission is reduced to just 15 dB. The multiple aluminium mounts reduce only a little the isolation capability of the single aluminium mount as can be seen from figures 5 and 18.

2. When two block masses are applied at each end of the rubber mounts an extra isolation effect is obtained which, by comparing figures 16 and 20, could be estimated to be about 18 dB at 1 kHz. Comparing this result with that obtained for the single mount shown in figure 7 it is evident that the passive isolation effectiveness of a single mount with block masses is similar to that of three mounts with block masses. The single mount isolation is few dB higher than that of the multiple mounts isolator. The isolation related to the inertial effect of block masses is increased by three times with the system with three mounts so that, although the increment of the number of mounts degrade the isolation due to structural damping effects, the global level of isolation of a single mount or three mount differs very little. Comparing figures 7 and 20 the single mount isolator seems to give about 5 dB higher isolation than the three mount isolator.

As seen for the single aluminium mount case, the presence of additional masses at the multiple aluminium mount isolator does not affect significantly the vibration transmission as can be determined by comparing figures 5 and 18.

3. In general the three control strategies under study, power minimisation and force or velocity cancellation, have given similar control effects.
4. Comparing the results of case 7 with those of case 6, no major differences have been detected when the reactive actuators are used in place of the inertial actuators.
5. The presence of block masses mounted at each end of the mounts do not produce significant effects on the control performances.
6. The rubber active isolators give very good control performance which, as shown by figures 17, 21 and 25, goes from a maximum of about 60 dB reduction at very low frequency to a minimum of a few dB at about 1 kHz. Comparing for example figure 8 with figure 21 it can be seen that the active isolation with either of the control strategies gives similar results for the single or the three mounts isolators.
7. Also the active isolator with three aluminium mounts gives very poor control performances which are of the order of few dB at very narrow frequency and can be considered negligible at the remaining frequencies.

Also for the multiple mounting system the isolation effectiveness has been assessed in a final case, case 8, of the system with rubber or aluminium mounts with lumped masses at the top and bottom ends ($W_t = 9.8 \times 10^{-3}$ Kg $W_b = 3.1 \times 10^{-3}$ Kg) and with an inertial control actuator modelled as sky hook force acting at the top end of the mount when the harmonic primary unit excitation is acting at position P_1, P_2 or P_3. Figure 28 shows that both the rubber and the aluminium isolator control capabilities are not affected by the position of the primary excitation.

CASE 5.

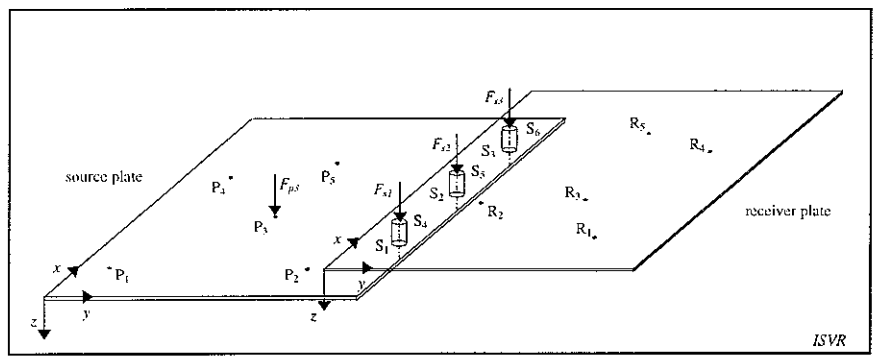

RUBBER

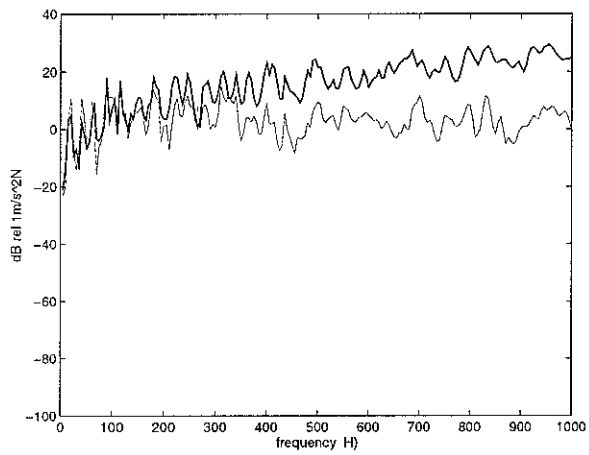

Figure 16: Estimate of the source K_{Es} (solid line) and receiver K_{Er} (faint) kinetic energy when the primary force F_{p3} is exciting the two panel system with three rubber mounts without block masses and an inertial control force.

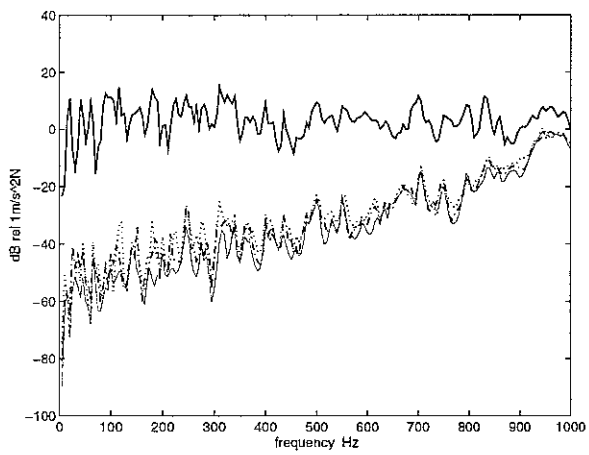

Figure 17: Estimate of the receiver K_{Er} kinetic energy when the primary force F_{p3} is exciting the two panel system with three rubber mounts without block masses and an inertial control force. Solid line, without control; faint line, when total power is minimised; dotted line, when forces are cancelled; dash-dotted line when velocities are cancelled.

ALUMINIUM

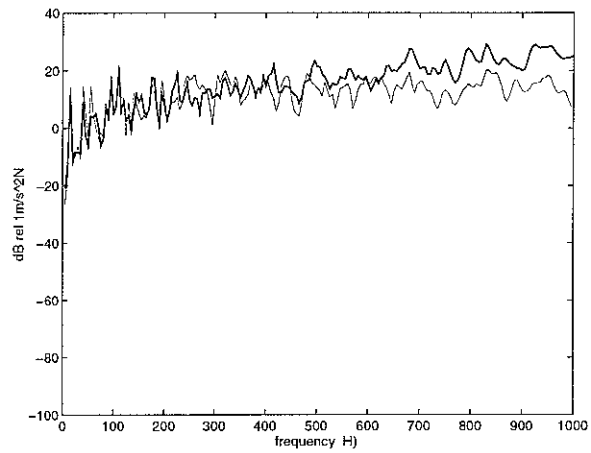

Figure 18: Estimate of the source K_{Es} (solid line) and receiver K_{Er} (faint) kinetic energy when the primary force F_{p3} is exciting the two panel system with three aluminium mounts without block masses and an inertial control force.

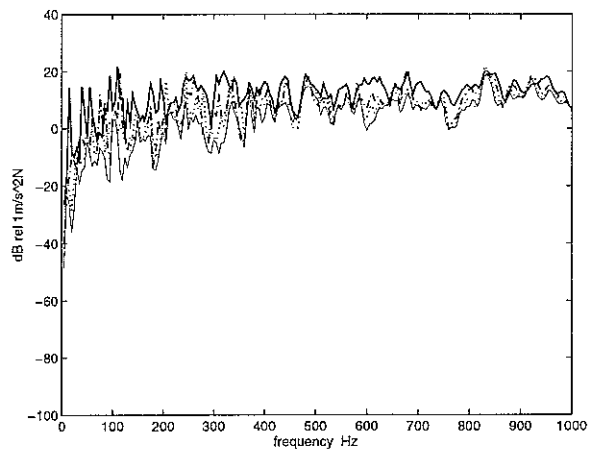

Figure 19: Estimate of the receiver K_{Er} kinetic energy when the primary force F_{p3} is exciting the two panel system with three aluminium mounts without block masses and an inertial control force. Solid line, without control; faint line, when total power is minimised; dotted line, when forces are cancelled; dash-dotted line when velocities are cancelled.

CASE 6.

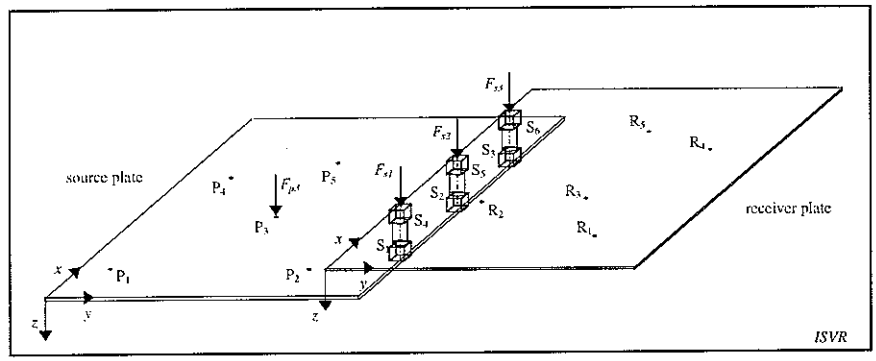

RUBBER

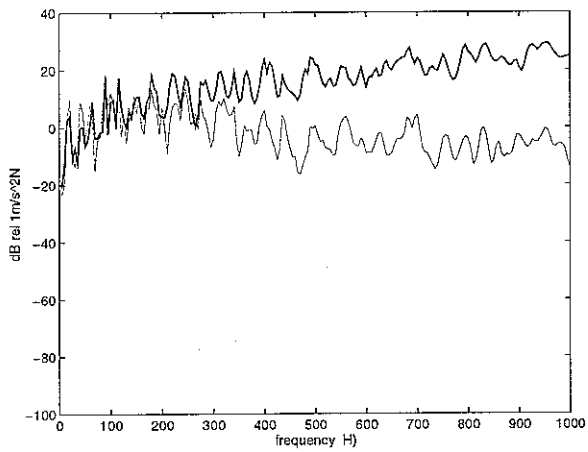

Figure 20: Estimate of the source K_{Es} (solid line) and receiver K_{Er} (faint) kinetic energy when the primary force F_{p3} is exciting the two panel system with three rubber mounts with block masses and an inertial control force.

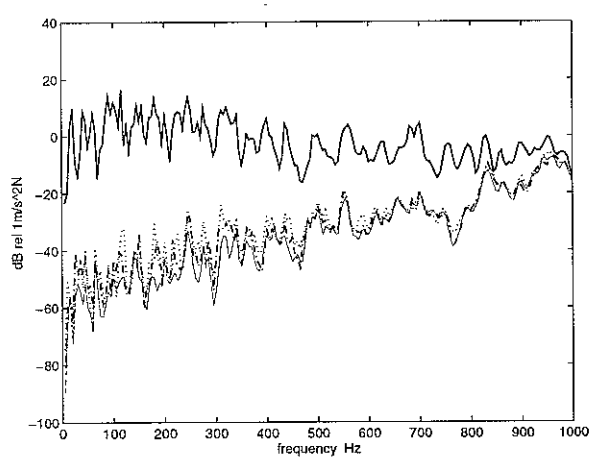

Figure 21: Estimate of the receiver K_{Er} kinetic energy when the primary force F_{p3} is exciting the two panel system with three rubber mounts with block masses and an inertial control force. Solid line, without control; faint line, when total power is minimised; dotted line, when forces are cancelled; dash-dotted line when velocities are cancelled.

ALUMINIUM

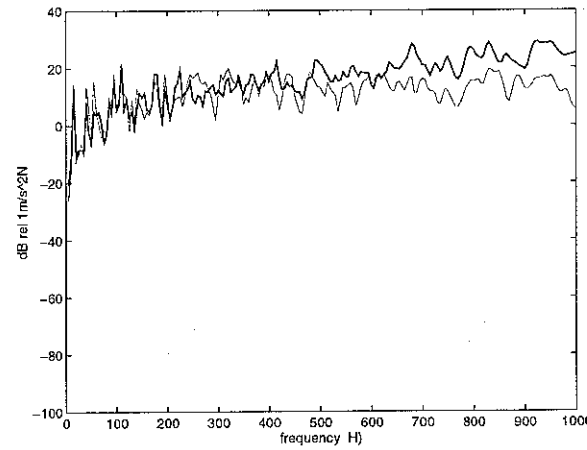

Figure 22: Estimate of the source K_{Es} (solid line) and receiver K_{Er} (faint) kinetic energy when the primary force F_{p3} is exciting the two panel system with three aluminium mounts with block masses and an inertial control force.

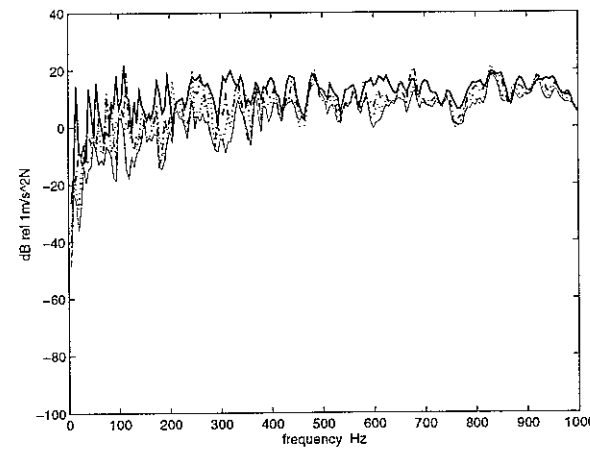

Figure 23: Estimate of the receiver K_{Er} kinetic energy when the primary force F_{p3} is exciting the two panel system with three aluminium mounts with block masses and an inertial control force. Solid line, without control; faint line, when total power is minimised; dotted line, when forces are cancelled; dash-dotted line when velocities are cancelled.

CASE 7.

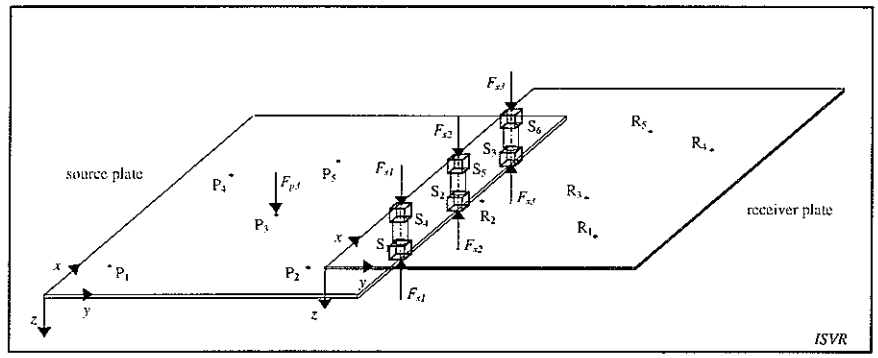

RUBBER

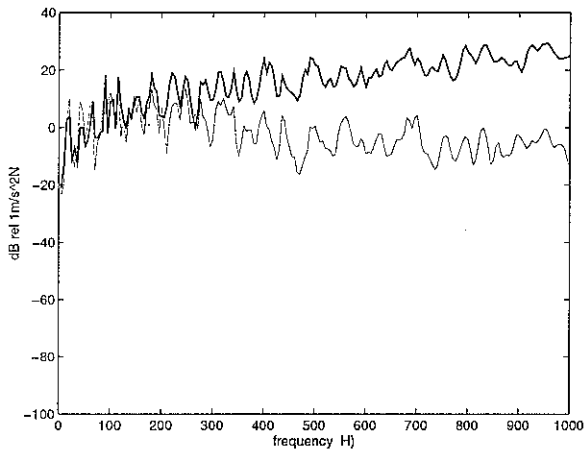

Figure 24: Estimate of the source K_{Es} (solid line) and receiver K_{Er} (faint) kinetic energy when the primary force F_{p3} is exciting the two panel system with three rubber mounts with block masses and a pair of reactive control forces.

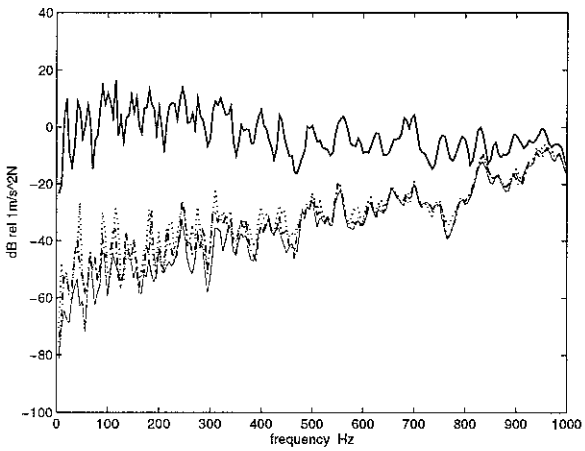

Figure 25: Estimate of the receiver K_{Er} kinetic energy when the primary force F_{p3} is exciting the two panel system with three rubber mounts with block masses and a pair of reactive control forces. Solid line, without control; faint line, when total power is minimised; dotted line, when forces are cancelled; dash-dotted line when velocities are cancelled.

ALUMINIUM

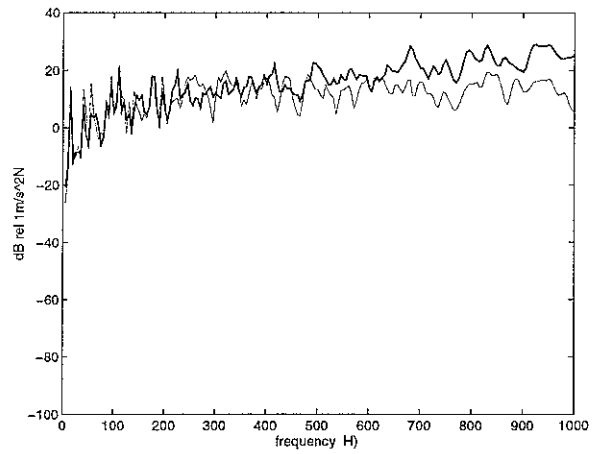

Figure 26: Estimate of the source K_{Es} (solid line) and receiver K_{Er} (faint) kinetic energy when the primary force F_{p3} is exciting the two panel system with three aluminium mounts with block masses and a pair of reactive control forces.

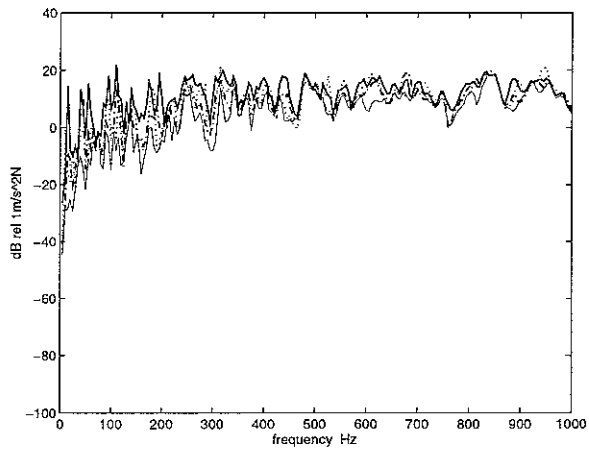

Figure 27: Estimate of the receiver K_{Er} kinetic energy when the primary force F_{p3} is exciting the two panel system with three aluminium mounts with block masses and a pair of reactive control forces. Solid line, without control; faint line, when total power is minimised; dotted line, when forces are cancelled; dash-dotted line when velocities are cancelled.

CASE 8.

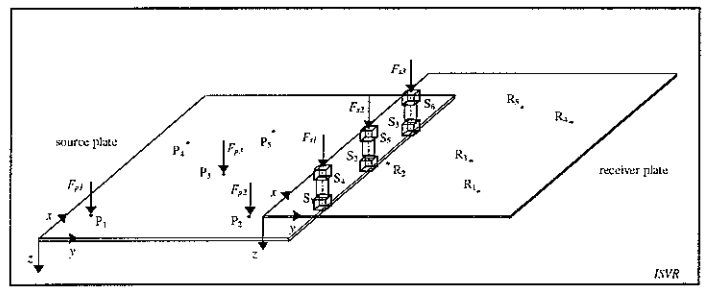

RUBBER **ALUMINIUM**

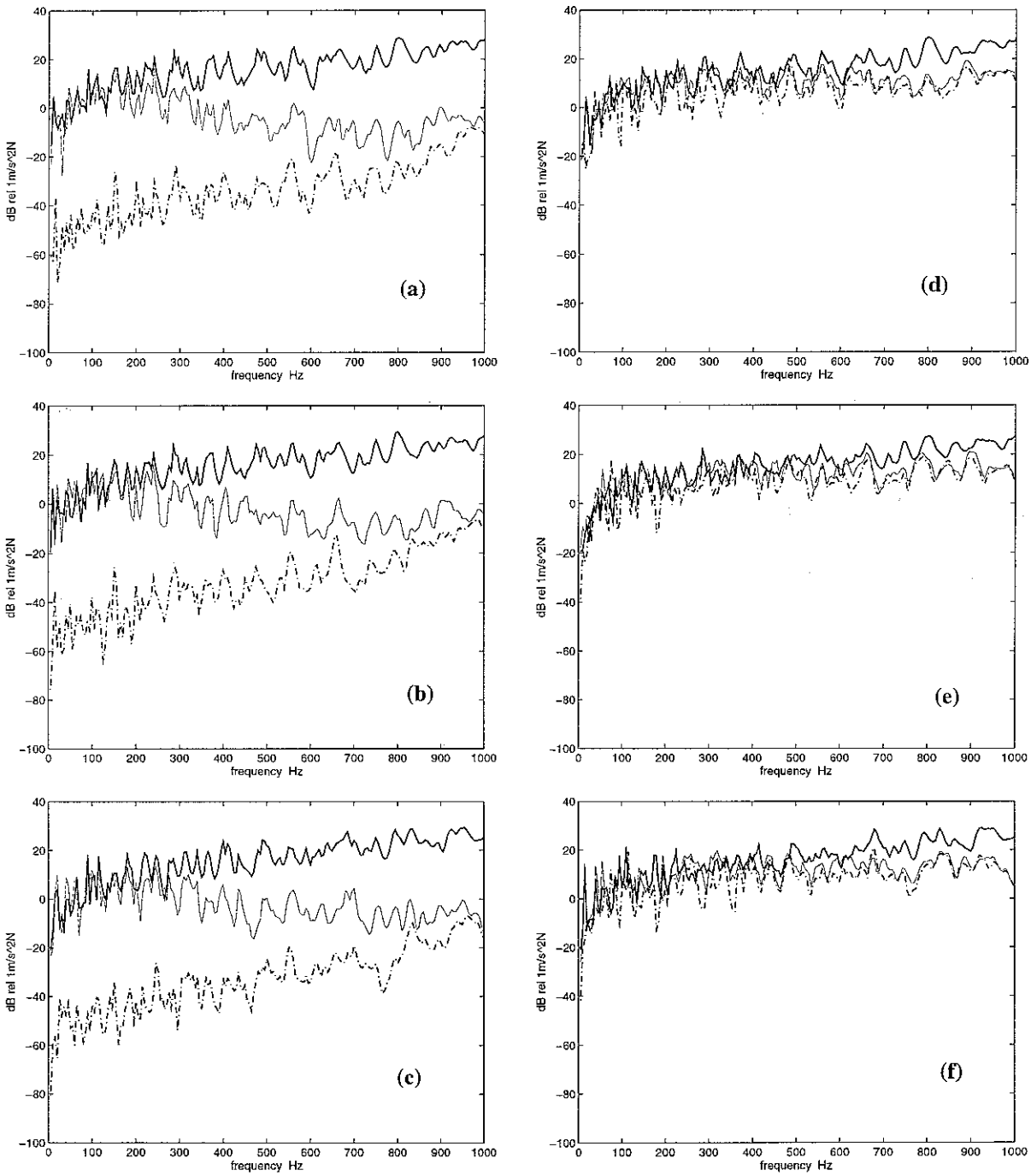

Figure 28: Estimate of the source K_{Es} kinetic energy (solid line) and receiver K_{Er} kinetic energy without (faint line) and with (dash-dotted line) active control when the primary force (a,d) F_{p1} (b,e) F_{p2} (c,f) F_{p3} is exciting the two panel system with either three rubber (cases a,b,c) or three aluminium (cases d,e,f) mounts with block masses and an inertial control force.

5.3 Effects due to block masses applied at each end of the mounts

The simulations carried out for the single and three mount isolators have shown that the block masses applied at each end of the mounts increase the passive isolation effectiveness. In this section the relation between the weight of these masses and the growth of the isolation has been assessed by considering the system studied in case 6 when the velocity control strategy is implemented and the masses listed in the following table are applied to each end of the three mounts

Tab 5: weights of the top and bottom masses

Case	W_T (Kg)	W_B (Kg)
a	0	0
b	$1.5\text{x}10^{-3}$	$5\text{x}10^{-3}$
c	$3.0\text{x}10^{-3}$	$10\text{x}10^{-3}$
d	$6.0\text{x}10^{-3}$	$20\text{x}10^{-3}$
e	$9.0\text{x}10^{-3}$	$30\text{x}10^{-3}$
f	$12.0\text{x}10^{-3}$	$40\text{x}10^{-3}$

The picture that can be drawn from figures 29 and 30 is that as the weight of the block masses rises as both the passive and active isolation tend to increase. The passive isolation increment is effective at frequencies above 250 Hz and tends to grow as the frequency rises. The active isolation effect is instead effective above 620 Hz and, as for the passive isolation, tends to grow as the frequency increase. Figure 29, bottom plot, shows that between 360 Hz and 440 Hz the trend described above is inverted for the active isolation case so that the isolation reduces as the weight of the masses increase.

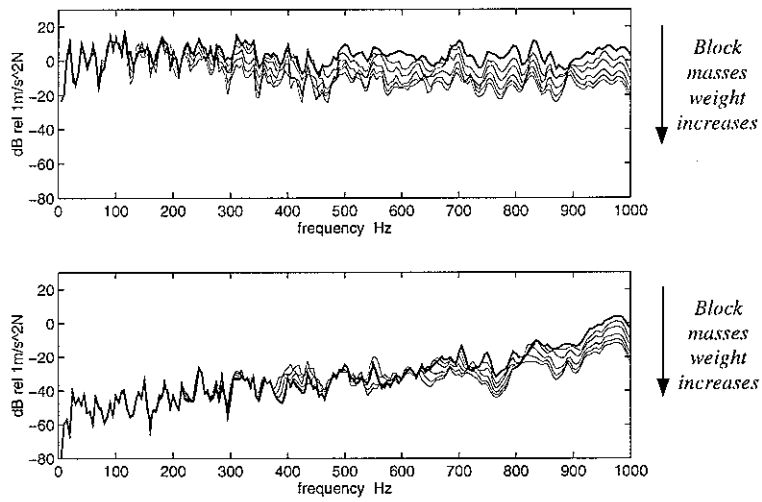

Figure 29: Estimate of the receiver K_{Er} kinetic energy without (top plot) and with (bottom plot) active control by means of the velocity control strategy when the primary force F_{p3} is exciting the two panels system.

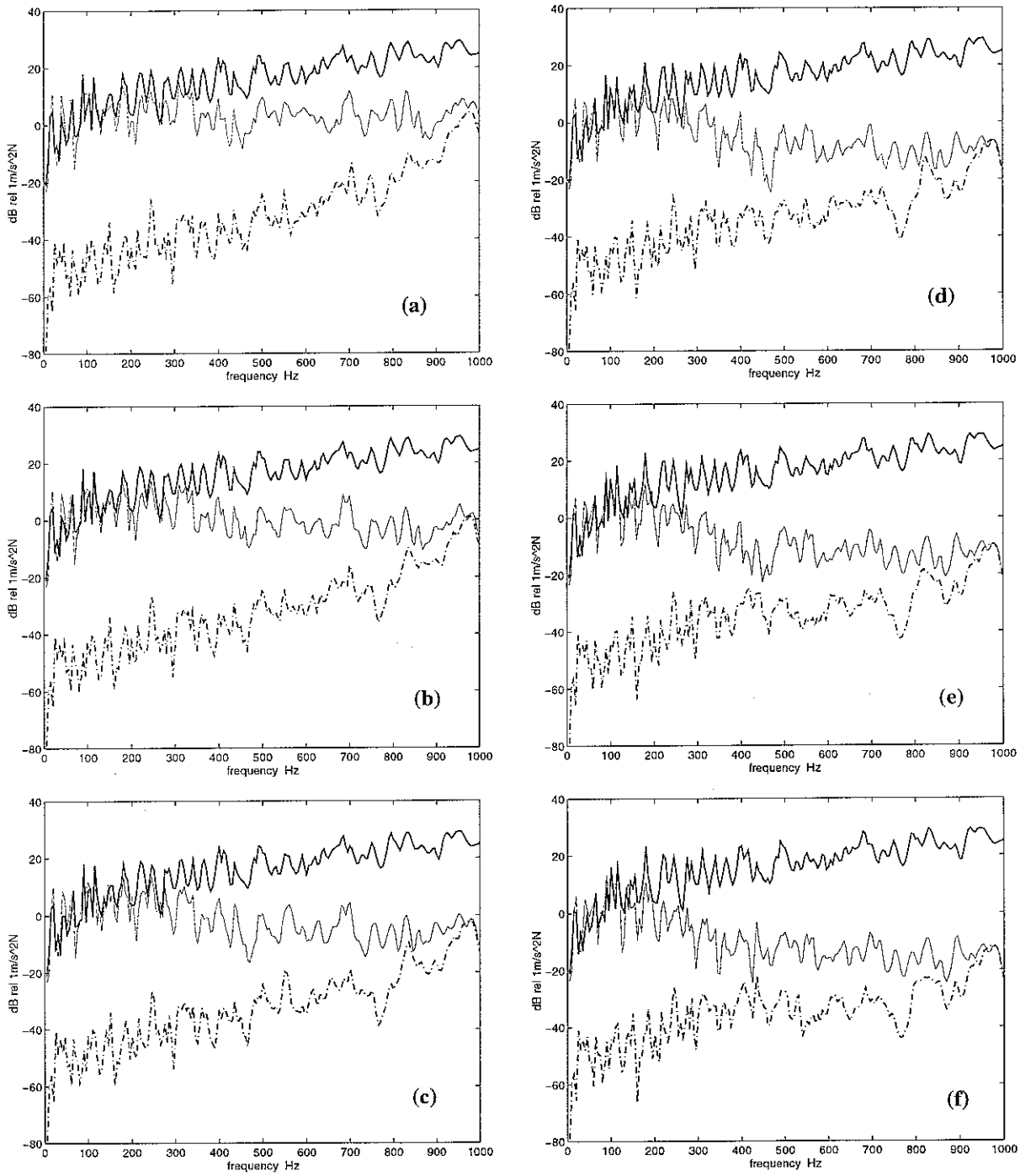

Figure 30: Estimate of the source K_{Es} kinetic energy (solid line) and receiver K_{Er} kinetic energy without (faint line) and with (dash-dotted line) active control when the velocity control strategy is implemented and the primary force F_{p3} is exciting the two panel system.

Case (a)	W_T=0	Kg	W_B=0	Kg
Case (b)	W_T=1.5x10^{-3}	Kg	W_B=5x10^{-3}	Kg
Case (c)	W_T=3.0x10^{-3}	Kg	W_B=10x10^{-3}	Kg
Case (d)	W_T=6.0x10^{-3}	Kg	W_B=20x10^{-3}	Kg
Case (e)	W_T=9.0x10^{-3}	Kg	W_B=30x10^{-3}	Kg
Case (f)	W_T=12.0x10^{-3}	Kg	W_B=40x10^{-3}	Kg

5.4 Effects related to the mounting system stiffness

The simulations carried out for the single and isolators with three mounts have also shown that the stiffness of the mounts affect both the passive and active isolation. The passive and active isolation when velocity cancellation is implemented has been evaluated with reference to the system of case 6 by considering a set of mounts whose density and stiffness has been chosen between two limiting cases: first, a very soft rubber mount and second, a relatively stiff aluminium mount as summarised in the following table.

Tab 6: Stiffness and density of the mounts

Case	E_m (N/m^2)	ρ_m (Kg/m^3)
a	$7.5\text{x}10^4$	648
b	$1.5\text{x}10^6$	1078
c	$2.9\text{x}10^7$	1508
d	$4.3\text{x}10^8$	1938
e	$5.8\text{x}10^9$	2368
f	$7.2\text{x}10^{10}$	2798

Considering the results shown in figures 31 and 32 it can be concluded that both the passive and active isolation tend to grow as the stiffness/density of the mounts decrease. Also, figure 32 shows that as the stiffness/density of the mounts increase as the active control benefits vanish so that passive and active isolation give similar results (see plots *d*, *e* and *f* of figure 32).

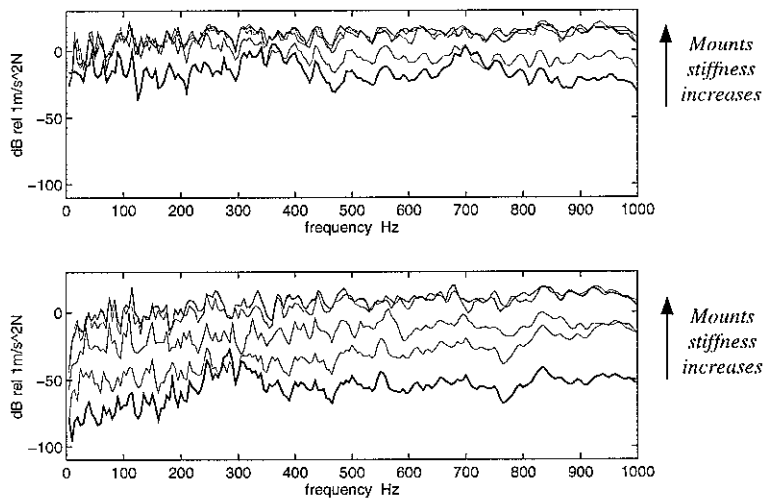

Figure 31: Estimate of the receiver K_{Er} kinetic energy without (top plot) and with (bottom plot) active control by means of the velocity control strategy when the primary force F_{p3} is exciting the two panel system.

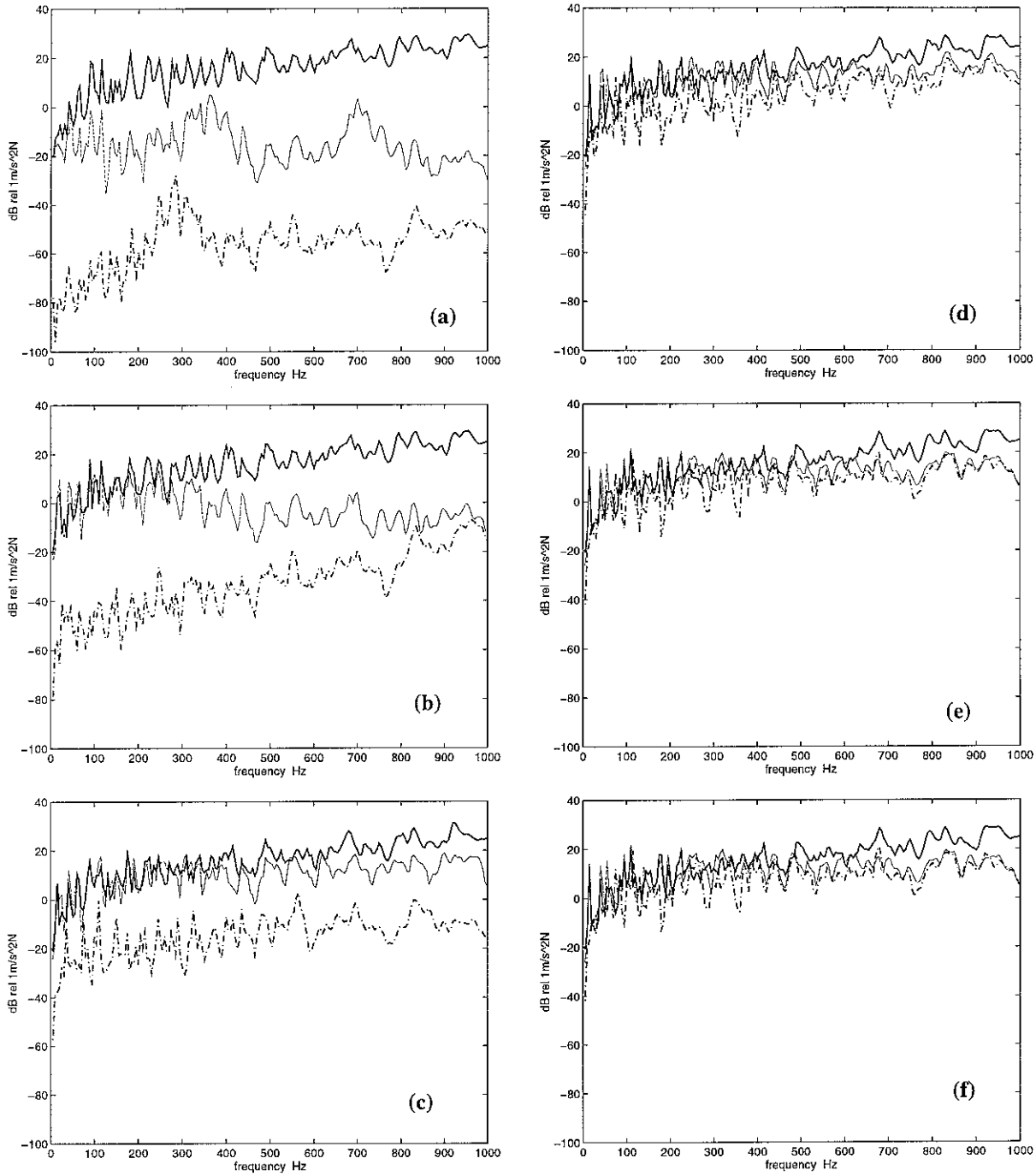

Figure 32: Estimate of the source K_{Es} kinetic energy (solid line) and receiver K_{Er} kinetic energy without (faint line) and with (dash-dotted line) active control when the primary force F_{p3} is exciting the two panel system.

Case (a)	E_m=7.5x10^4 N/m^2	ρ_m=648 Kg/m^3
Case (b)	E_m=1.5x10^6 N/m^2	ρ_m=1078 Kg/m^3
Case (c)	E_m=2.9x10^7 N/m^2	ρ_m=1508 Kg/m^3
Case (d)	E_m=4.3x10^8 N/m^2	ρ_m=1938 Kg/m^3
Case (e)	E_m=5.8x10^9 N/m^2	ρ_m=2368 Kg/m^3
Case (f)	E_m=7.2x10^{10} N/m^2	ρ_m=2798 Kg/m^3

5.5 Comparison between IMM simulations and SEA and experimental results

The impedance-mobility matrix model IMM described and used in this report has been tested by comparing the results it produces with three different types of analysis carried out for the AIRAT project by DERA [28,29]: first, a statistical energy analysis SEA; second, a matrix analysis which uses measured transfer functions between the primary and control excitation positions and the control positions at the mount junctions and the monitoring positions on the receiver panel MTF and third, a fully experimental analysis carried out at a set of 24 tones between 110 Hz and 340 Hz EA.

The comparison has been carried out for the two plate system shown in figure 2 having either a rubber or aluminium mount with lumped masses at the top and bottom ends ($W_t = 9.8\times10^{-3}$ Kg $W_b = 3.1\times10^{-3}$ Kg) and with inertial control actuators acting at the top end of the mounts. The control strategy tested was the cancellation of axial velocities at the top of the mounts. The primary excitation has been chosen at position P_3 . Figures 33 and 34 shows the estimate of the receiver K_{Er} kinetic energy without (top plot) and with (bottom plot) active control for the two types of isolator systems.

In both cases, rubber and aluminium isolators, very good agreement has been obtained between the four type of predictions without control (top plots).

Also the comparison between the four types of predictions with control are quite satisfying. The IMM simulations agree quite well with both the experimental results, SEA, and with the matrix approach based on measured transfer functions MTF. Below 150 Hz there are some discrepancies between the IMM and the MTF predictions which are probably due to the fact that the experimental transfer functions used by the MTF approach are not reliable below 100 Hz [28]. Also, the bottom plot of figure 34 shows that when the aluminium isolator is used there is a mismatching of about 10 dB in a frequency range between 520 Hz, and 980 Hz between the predictions with the IMM model and those obtained from the MFT method. The method using measured transfer functions, MTF, predicts larger active isolation than that of the analytical model IMM. This could be due to the non perfect alignment of the mounts in the experimental rig, so that a larger control effectiveness is predicted, since the experimental control system is able to reduce not only the vibration transmission due to axial vibration of the mounts but also the vibration transmission related to the angular vibrations of the mounts.

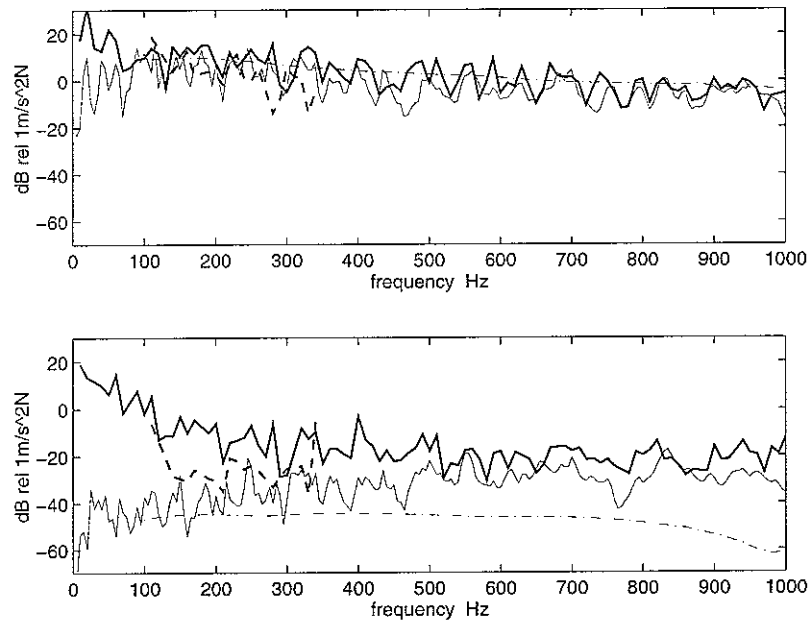

Figure 33: Estimate of the receiver K_{Er} kinetic energy without (top plot) and with (bottom plot) active control of the out-of-plane velocities at the receiver mounts junction when the primary force F_{p3} is exciting the two panel system with three rubber mounts having block masses at the ends. Solid line: MTF predictions, faint line: IMM predictions, dash-dotted line: SEA predictions, dashed line: EA predictions

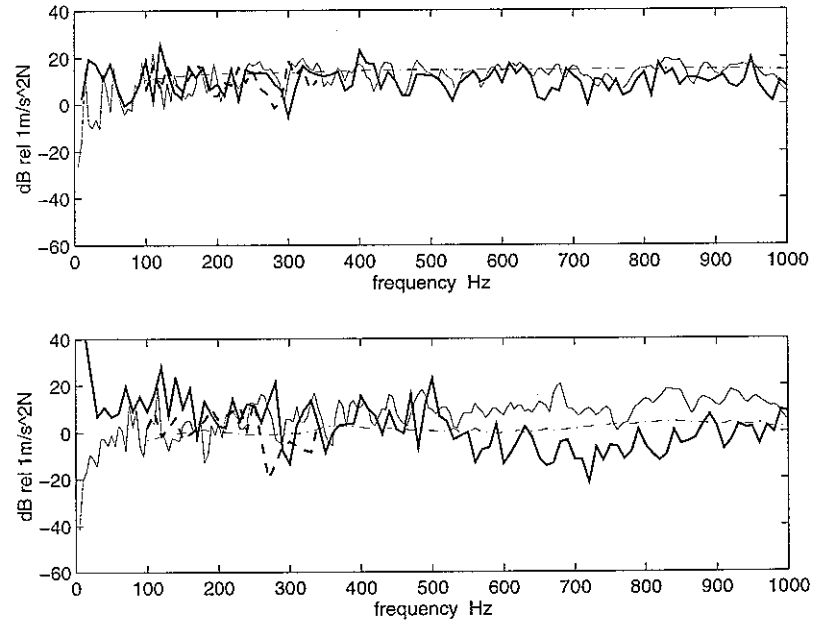

Figure 34: Estimate of the receiver K_{Er} kinetic energy without (top plot) and with (bottom plot) active control of the out-of-plane velocities at the receiver mounts junction when the primary force F_{p3} is exciting the two panel system with three aluminium mounts having block masses at the ends. Solid line: MTF predictions, faint line: IMM predictions, dash-dotted line: SEA predictions, dashed line: EA predictions

6. CONCLUSIONS

The study presented in this report is part of a collaborative research program whose acronym is AIRAT: "Active Isolator Research for Aircraft Trim Panels". The main goal of the project is to study and develop an active mounting system for the trim panels mounted in aircraft or helicopters in order to reduce the sound transmission to the cabin.

This report introduces the theory of an impedance-mobility matrix model used to predict the structural vibration transmission between two plates coupled via an active mounting system. The two plates are assumed acoustically uncoupled. With this model the active and passive isolation effectiveness of different types of mounting systems have been studied; in particular, the case of a single or a three mount isolator system with inertial actuators applied at the top end of the mounts has been investigated in order to assess the effects generated by the stiffness of the mounts and the effects produced by the rigid elements (block masses) present at each end of the mounts.

Three cost functions have been investigated: first, the minimisation of the total structural power transmitted by the source to the receiver; second, the cancellation of out-of-plane input velocities to the receiver and the cancellation of out-of-plane input forces to the receiver.

The main conclusions of the study presented can be summarised by the following points.

1. The rubber mount isolator provides better passive isolation effects than that with aluminium mounts.
2. The use of multiple mounts does not increase the passive isolation performance, on the contrary it degrades the isolation potentiality of the single mount.
3. When two block masses are applied at the each end of the rubber mounts an extra isolation effect is obtained. This effect is negligible when aluminium mounts are used.
4. The three control strategies under study have given similar active control effectiveness in all cases examined.
5. No major differences have been found when the reactive actuators are used in place of the inertial actuators.
6. The presence of block masses mounted at each end of the mounts do not produce significant effects on the active control performances of both rubber and aluminium mounts.
7. The rubber active isolators give very good active control performance which goes from a maximum of about 60 dB reduction at very low frequency to a minimum of few dB at about 1 kHz while the active isolator with aluminium mounts gives very poor control performances.

The model used and described in this report has been validated with data given by three other methods: first, an analytical method based on a statistical energy analysis approach; second a matrix method based on measured transfer functions and third, an experimental method which considered real time active control for tonal excitations.

7. FUTURE WORK

The simplification of the matrix model (no account has been taken of mount axial stiffness correction factor μ for resilient mount made of rubber or the vibratory contribution of in plane components) seems to be acceptable for the passive vibration transmission analysis. However, the results obtained when control forces are acting on the system do not match so well with experimental ones. It is therefore recommended to further

investigate this model of the dynamics of the system with particular attention to the modelling of the vibration transmission by the mounting system.

8. ACKNOWLEDGEMENTS

Although the mathematical model described here was mainly developed under other funding, the rest of the work reported here was supported by the Aero-Structures Department at DERA Farnborough, and in particular the support and collaboration of Professor K. Heorn and Mr R. Harris is gratefully acknowledged.

9. REFERENCES

[1] Crede C.E. and Ruzicka J.E. (1976). *Theory of vibration isolation.* Chapter 30 of *Shock and Vibration Handbook*, Edited by Harris C.M. and Crede C.E. McGraw-Hill New York.

[2] Petit (1998). *Introduction to finite element vibration analysis.* Cambridge University (2nd edition).

[3] Lyon R.H. and DeJong R.G. (1995), *Theory and application of statistical energy analysis.* Butterworth-Heinemann Oxford, second edition.

[4] Gardonio P., Elliott S.J., and Pinnington R.J. (1997). Active isolation of structural vibration on multiple-degree-of-freedom system. Part I: dynamic of the system, *Journal of Sound and Vibration*, **207**(1).

[5] Skudrzyk E. (1959). Theory of noise and vibration insulation of a system with many resonances. *The Journal of the Acoustical Society of America*, **31**(1), 68-74.

[6] Snowdon J.C. (1961). Reduction of the response to vibration of structures possesing finite mechanical impedance. *Journal of the Acoustical Society of America* **33**(11), 1466-1475.

[7] Snowdon J.C. (1962). Isolation from vibration with a mounting utilizing low- and high-damping rubberlike materials. *Journal of the Acoustical Society of America* **34**(1), 54-61.

[8] Rubin S. (1964). Transmission matrices for vibration and their relation to admittance and impedance. *Transaction of the ASME Journal of Engineering for Industry*, **86**(1), 9-21.

[9] Snowdon J.C. (1965). Rubberlike materials, their internal damping and role in vibration isolation. *Journal of Sound and Vibration* **2**(2), 175-193.

[10] Ungar E.E. and Dietrich C.W. (1966). High-frequency vibration isolation. *Journal of Sound and Vibration*, **4**(2), 224-241.

[11] Rubin S. (1967). Mechanical immitance- and transmission-matrix concepts. *Journal of the Acoustical Society of America*, **41**(5), 1171-1179.

[12] Rubin S. (1967). Mechanical impedance approach to engine vibration transmission into an aircraft fuselage. Proceedings of *Aeronautic & Space Engineering and Manufacturing Meeting*, Los Angeles, CA, 2-6 October 1967.

[13] Soliman J.I. and Hallam M.G. (1968). Vibration isolation between non-rigid machines and non-rigid foundations. *Journal of Sound and Vibration*, **8**(2), 329-351.

[14] Snowdon J.C. (1971). Mechanical four-pole parameters and their application. *Journal of Sound and Vibration* **15**(3), 307-323.

[15] Munjal M.L. (1975). A rational synthesis of vibration isolators. *Journal of Sound and Vibration*, **39**(2), 247-263.

[16] Petersson B. and Plunt J. (1982). On effective mobilities in the prediction of structure-borne sound transmission between a source structure and a receiving structure, part I theoretical background and basic experimental studies *Journal of Sound and Vibration*, **82**(4), 517-529.

[17] Gordis J.H., Bielawa R.L. and Flannelly W.G. (1991). A general theory for frequency domain structural synthesis. *Journal of Sound and Vibration*, **150**(1), 139-158.

[18] Swanson D.A., Miller L.R. and Norris M.A. (1994). Multidimensional mount effectiveness for vibration isolation. *Journal of Aircraft*, **31**(1), 188-196.

[19] Goyder H.G.D. and White R.G. (1980). Vibrational power flow from machines into built-up structures, part I: introduction and approximate analyses of beam and plate-like foundations. *Journal of Sound and Vibration* **68**(1), 59-75.

[20] Pinnington R.J. White R.G. (1980). Power flow through machine isolators to resonant and non-resonant beams. *Journal of Sound and Vibration* **75**(1),179-197.

[21] Pinnington R.J. (1987). Vibrational Power Transmission to a Seating of a Vibration Isolated Motor. *Journal of Sound and Vibration* **118**(3), 515-530.

[22] Pinnington R.J. (1990). Vibrational power transmission from a finite source beam to an infinite receiver beam via a continuous compliant mount. *Journal of Sound and Vibration* **137**(1), 117-129.

[23] Pan Jie, Pan Jiaqiang and Hansen C.H. (1992). Total power flow from a vibrating rigid body to a thin panel through multiple elastic mounts. *Journal of the Acoustical Society of America* **92**(2), 895-907.

[24] Farstad J.E. and Singh R. (1995). Structurally transmitted dynamic power in discretely joined damped component assemblies. *Journal of the Acoustical Society of America* **97**(5), 2855-2865.

[25] Rook T.E. and Singh R. (1995). Power flow through multidimensional compliant joints using mobility and modal approaches. *Journal of the Acoustical Society of America* **97**(5), 2882-2891.

[26] Gardonio P. and Elliott S.J., (1998). A comparison of active control strategies for the reduction of structural vibration transmission, Proceedings of *The Fourth International Conference on Motion and Vibration Control (MOVIC)*, ETH Zurich, CH, 25-28 August 1998, 503-508.

[27] Fuller C.R., Elliott S.J. and Nelson P.A. (1997). *Active Control of Vibration*, Academic Press, London.

[28] Harris R.I. (1998). Active isolator research for aircraft trim panels: experiments with 3 isolators. *Defence Evaluation and Research Agency, Farnborough Hempshire UK, internal report* No. DERA/AS/ASD/TR980154/1.0

[29] Heron K.H. (1998). Predictive statistical energy analysis and collocated active control. *Defence Evaluation and Research Agency, Farnborough Hempshire UK, internal report* No. DERA/MSS5/TR980720

[30] Gardonio P. and Elliott S.J. (1998). Driving point and transfer mobility matrices for thin plates excited in flexure. *ISVR Technical Report* No 277 (*University of Southampton, Southampton UK*).

[31] Cremer L., Heckl M. and Ungar E.E. (1988). *Structure-Borne Sound.* Springer-Verlag Berlin Heidelberg New York 1988, (second edition).

[32] Bishop, R.E.D. and Johnson, D.C. (1960). *The Mechanics of Vibration.* Cambridge at the University Press Cambridge.

[33] O'Hara, G.J. (1966). Mechanical impedance and mobility concepts. *Journal of the Acoustical Society of America* **41**(5), 1180-1184.

APPENDIX A: PLATES MOBILITY MATRICES.

The mobility matrices used into equations (53), (54) (57) and (58) have been derived using modal formulae for the point and transfer mobility terms of a plate excited only in bending as from reference [30].

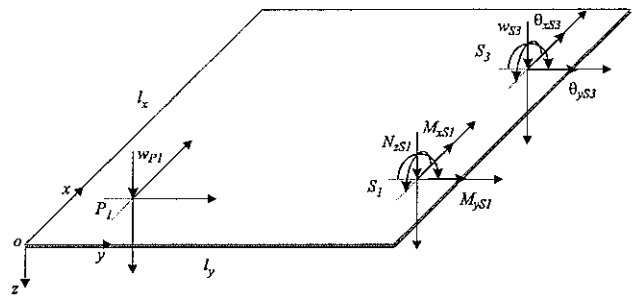

Figure A1: *Notation of the displacement w at positions P_1 and S_3, and of the rotations θ_x, and θ_y, at positions S_3 when a plate is excited in flexure by a point force N_z and point moments M_x, and M_y, at position S_1*

The sub-mobility matrix between two generic positions, for example between positions S_3 and S_1 (see figure A1) of the source plate is defined as follow:

$$\mathbf{M}_{S3S1}(\omega)=\begin{bmatrix} M_{wNz}^{S3S1}(\omega) & M_{wMx}^{S3S1}(\omega) & M_{wMy}^{S3S1}(\omega) \\ M_{\theta xNz}^{S3S1}(\omega) & M_{\theta xMx}^{S3S1}(\omega) & M_{\theta xMy}^{S3S1}(\omega) \\ M_{\theta yNz}^{S3S1}(\omega) & M_{\theta yNz}^{S3S1}(\omega) & M_{\theta yMy}^{S3S1}(\omega) \end{bmatrix} \tag{A1}$$

where assuming the harmonic motion with time dependence of the form $\exp(j\omega t)$ and according to reference [30] the individual mobility terms are given by the following modal formulae:

$$M_{wNz}^{S3S1}(\omega)=\frac{\tilde{\dot{w}}_{S3}(\omega)}{\tilde{N}_{zS1}(\omega)}=j\omega\sum_{m=1}^{\infty}\sum_{n=1}^{\infty}\frac{\phi_{mn}(S_3)\phi_{mn}(S_1)}{\Lambda_{mn}\left[\omega_{fmn}^2(1+j\eta)-\omega^2\right]}\ ; \tag{A2}$$

$$M_{wMx}^{S3S1}(\omega)=\frac{\tilde{\dot{w}}_{S3}(\omega)}{\tilde{M}_{xS1}(\omega)}=j\omega\sum_{m=1}^{\infty}\sum_{n=1}^{\infty}\frac{\phi_{mn}(S_3)\psi_{mn}^{(x)}(S_1)}{\Lambda_{mn}\left[\omega_{fmn}^2(1+j\eta)-\omega^2\right]}\ ; \tag{A3}$$

$$M_{wMy}^{S3S1}(\omega)=\frac{\tilde{\dot{w}}_{S3}(\omega)}{\tilde{M}_{yS1}(\omega)}=j\omega\sum_{m=1}^{\infty}\sum_{n=1}^{\infty}\frac{\phi_{mn}(S_3)\psi_{mn}^{(y)}(S_1)}{\Lambda_{mn}\left[\omega_{fmn}^2(1+j\eta)-\omega^2\right]}\ ; \tag{A4}$$

$$M_{\theta xNz}^{S3S1}(\omega)=\frac{\tilde{\dot{\theta}}_{xS3}(\omega)}{\tilde{N}_{zS1}(\omega)}=j\omega\sum_{m=1}^{\infty}\sum_{n=1}^{\infty}\frac{\psi_{mn}^{(x)}(S_3)\phi_{mn}(S_1)}{\Lambda_{mn}\left[\omega_{fmn}^2(1+j\eta)-\omega^2\right]}\ ; \tag{A5}$$

$$M_{\theta yNz}^{S3S1}(\omega)=\frac{\tilde{\dot{\theta}}_{yS3}(\omega)}{\tilde{N}_{zS1}(\omega)}=j\omega\sum_{m=1}^{\infty}\sum_{n=1}^{\infty}\frac{\psi_{mn}^{(y)}(S_3)\phi_{mn}(S_1)}{\Lambda_{mn}\left[\omega_{fmn}^2(1+j\eta)-\omega^2\right]}\ ; \tag{A6}$$

$$M_{\theta xMx}^{S3S1}(\omega)=\frac{\tilde{\dot{\theta}}_{xS3}(\omega)}{\tilde{M}_{xS1}(\omega)}=j\omega\sum_{m=1}^{\infty}\sum_{n=1}^{\infty}\frac{\psi_{mn}^{(x)}(S_3)\psi_{mn}^{(x)}(S_1)}{\Lambda_{mn}\left[\omega_{fmn}^2(1+j\eta)-\omega^2\right]}\ ; \tag{A7}$$

$$M_{\theta xMy}^{S3S1}(\omega)=\frac{\tilde{\dot{\theta}}_{xS3}(\omega)}{\tilde{M}_{yS1}(\omega)}=j\omega\sum_{m=1}^{\infty}\sum_{n=1}^{\infty}\frac{\psi_{mn}^{(x)}(S_3)\psi_{mn}^{(y)}(S_1)}{\Lambda_{mn}\left[\omega_{fmn}^2(1+j\eta)-\omega^2\right]}\ ; \tag{A8}$$

$$M_{\theta yMx}^{S3S1}(\omega)=\frac{\tilde{\dot{\theta}}_{yS3}(\omega)}{\tilde{M}_{xS1}(\omega)}=j\omega\sum_{m=1}^{\infty}\sum_{n=1}^{\infty}\frac{\psi_{mn}^{(y)}(S_3)\psi_{m,n}^{(x)}(S_1)}{\Lambda_{mn}\left[\omega_{fmn}^2(1+j\eta)-\omega^2\right]}\ ; \tag{A9}$$

$$M_{\theta yMy}^{S3S1}(\omega)=\frac{\tilde{\dot{\theta}}_{yS3}(\omega)}{\tilde{M}_{yS1}(\omega)}=j\omega\sum_{m=1}^{\infty}\sum_{n=1}^{\infty}\frac{\psi_{mn}^{(y)}(S_3)\psi_{m,n}^{(y)}(S_1)}{\Lambda_{mn}\left[\omega_{fmn}^2(1+j\eta)-\omega^2\right]}\ ; \tag{A10}$$

where ω is the circular frequency (rad/s) and η is the loss factor. The symbol "~" indicates a complex value whose absolute value and phase denotes respectively the amplitude and phase of the harmonic variation in time at the driving frequency ω of the linear/angular velocity and force/moment excitation terms. A detailed description on how to calculate the natural frequencies ω_{mn}, modal amplitudes ϕ_{mn}, modal slopes $\psi_{m,n}^{(x)}$, $\psi_{mn}^{(y)}$ and Λ_{mn} normalisation factor for a freely supported thin plate can be found in reference [30] (sec. 3.7).

The mobility matrix of equations (57) and (58) relates only the out-of-plane velocity component $\dot{w}_j$ at the five monitoring positions of the source and receiver plates to the mounting junctions positions force and moment parameters, therefore the sub-mobility matrix between a monitoring position and a mounting junction position, for example between positions P_1 and S_1 of the source plate, is defined as follow:

$$\mathbf{M}_{P1S1}(\omega)=\left[M_{wNz}^{P1S1}(\omega)\quad M_{wMx}^{P1S1}(\omega)\quad M_{wMy}^{P1S1}(\omega)\right]. \tag{A11}$$

APPENDIX B: MOUNTING SYSTEM IMPEDANCE AND EXCITATION MATRICES.

The impedance matrix used into equations (55) and (56) has been derived by modelling each mount as a distributed one dimensional element on which longitudinal and bending waves propagate. The impedance terms have been calculated by deriving the exact solution in closed form of the standard second order wave equation of longitudinal waves and of the Euler-Bernoulli fourth order wave equation of flexural waves [31], assuming the beam element either with both ends freely suspended or both ends pinned in x and y directions.

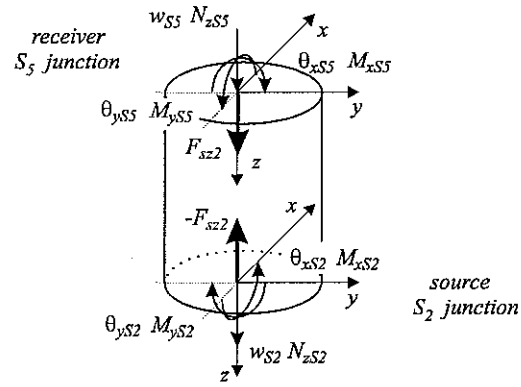

Figure B1: *Notation of the displacement w and rotations θ_x, and θ_y, point force N_z and point moments M_x, and M_y at the top and bottom junctions of mount number 2 of the system shown in figure 2.*

As discussed in section 3, it has been chosen to neglect three degrees of freedom at each mount junction. The following kinematic and dynamic parameters are not taken into account in the matrix formulation: first, the angular velocity and moment in z direction, $\dot{\theta}_z$ and M_z; second, the linear velocity and force in x direction, $\dot{u}$ and N_x, and third, the linear velocity and force in y direction, $\dot{v}$ and N_y. Therefore, at each end of the mounts only the linear velocity $\dot{w}$ and angular velocities, $\dot{\theta}_x$ and $\dot{\theta}_y$, and only the point force N_z and point moments, M_x and M_y, are accounted for. Figure B1 shows the notation of these three kineamtic and dynamic parameters at the top and bottom junctions of the mount number 2 whose junctions are denoted by the symbols S_2 (bottom junction) and S_5 (top junction).

If all six kinematic and dynamic parameters are accounted for at each end of a freely suspended mount element, the 12×12 impedance matrix would be defined as in the following relation:

$$\begin{Bmatrix} N_{xS2} \\ N_{yS2} \\ N_{zS2} \\ M_{xS2} \\ M_{yS2} \\ M_{zS2} \\ N_{xS5} \\ N_{yS5} \\ N_{zS5} \\ M_{xS5} \\ M_{yS5} \\ M_{zS5} \end{Bmatrix} = \begin{bmatrix} Z_{Nxu}^{S2S2} & 0 & 0 & 0 & Z_{Nx\theta y}^{S2S2} & 0 & Z_{Nxu}^{S2S5} & 0 & 0 & 0 & Z_{Nx\theta y}^{S2S5} & 0 \\ 0 & Z_{Nyv}^{S2S2} & 0 & Z_{Ny\theta x}^{S2S2} & 0 & 0 & 0 & Z_{Nyv}^{S2S5} & 0 & Z_{Ny\theta x}^{S2S5} & 0 & 0 \\ 0 & 0 & Z_{Nzw}^{S2S2} & 0 & 0 & 0 & 0 & 0 & Z_{Nzw}^{S2S5} & 0 & 0 & 0 \\ 0 & Z_{Mxv}^{S2S2} & 0 & Z_{Mx\theta x}^{S2S2} & 0 & 0 & 0 & Z_{Mxv}^{S2S5} & 0 & Z_{Mx\theta x}^{S2S5} & 0 & 0 \\ Z_{Myu}^{S2S2} & 0 & 0 & 0 & Z_{My\theta y}^{S2S2} & 0 & Z_{Myu}^{S2S5} & 0 & 0 & 0 & Z_{My\theta y}^{S2S5} & 0 \\ 0 & 0 & 0 & 0 & 0 & Z_{Mz\theta z}^{S2S2} & 0 & 0 & 0 & 0 & 0 & Z_{Mz\theta z}^{S2S5} \\ Z_{Nxu}^{S5S2} & 0 & 0 & 0 & Z_{Nx\theta y}^{S5S2} & 0 & Z_{Nxu}^{S5S5} & 0 & 0 & 0 & Z_{Nx\theta y}^{S5S5} & 0 \\ 0 & Z_{Nyv}^{S5S2} & 0 & Z_{Ny\theta x}^{S5S2} & 0 & 0 & 0 & Z_{Nyv}^{S5S5} & 0 & Z_{Ny\theta y}^{S5S5} & 0 & 0 \\ 0 & 0 & Z_{Nzw}^{S5S2} & 0 & 0 & 0 & 0 & 0 & Z_{Nzw}^{S5S5} & 0 & 0 & 0 \\ 0 & Z_{Mxv}^{S5S2} & 0 & Z_{Mx\theta x}^{S5S2} & 0 & 0 & 0 & Z_{Mxv}^{S5S5} & 0 & Z_{Mx\theta x}^{S5S5} & 0 & 0 \\ Z_{Myu}^{S5S2} & 0 & 0 & 0 & Z_{My\theta y}^{S5S2} & 0 & Z_{Myu}^{S5S5} & 0 & 0 & 0 & Z_{My\theta y}^{S5S5} & 0 \\ 0 & 0 & 0 & 0 & 0 & Z_{Mz\theta z}^{S5S2} & 0 & 0 & 0 & 0 & 0 & Z_{Mz\theta z}^{S5S5} \end{bmatrix} \begin{Bmatrix} \dot{u}_{S2} \\ \dot{v}_{S2} \\ \dot{w}_{S2} \\ \dot{\theta}_{xS2} \\ \dot{\theta}_{yS2} \\ \dot{\theta}_{zS2} \\ \dot{u}_{S5} \\ \dot{v}_{S5} \\ \dot{w}_{S5} \\ \dot{\theta}_{xS5} \\ \dot{\theta}_{yS5} \\ \dot{\theta}_{zS5} \end{Bmatrix} \quad \text{(B1)}$$

where the six kinematic (linear and angular velocities) and dynamic (force and moment excitations) parameters at each end of the mount are oriented as in the figure shown below.

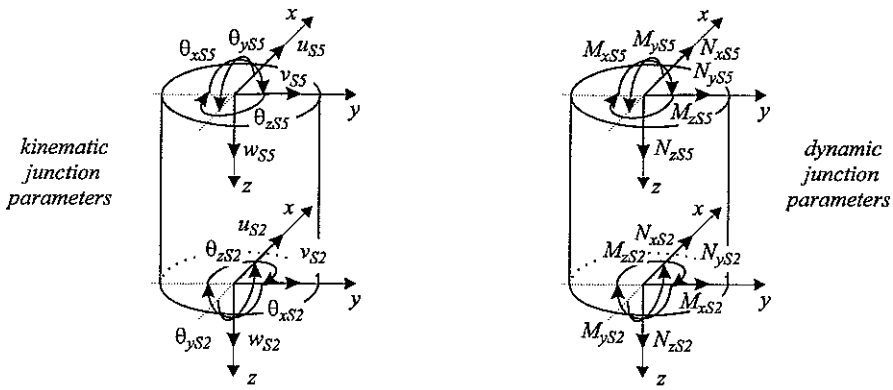

Figure B2: *Notation of the six kinematic (linear and angular displacements) and dynamic (force and moment excitations) parameters at each end of mount number 2 of the system shown in figure 2.*

The four impedance matrices $\mathbf{Z}_{11}$, $\mathbf{Z}_{12}$, $\mathbf{Z}_{21}$ and $\mathbf{Z}_{22}$ to be used into equations (55) and (56) can be obtained from the impedance matrix of equation (B.1) by removing the rows and columns for to the degrees-of-freedom neglected. Therefore,

$$\mathbf{Z}_{11} = \begin{bmatrix} \overline{Z}_{Nzw}^{S2S2} & 0 & 0 \\ 0 & \overline{Z}_{Mx\theta x}^{S2S2} & 0 \\ 0 & 0 & \overline{Z}_{My\theta y}^{S2S2} \end{bmatrix} \qquad \mathbf{Z}_{12} = \begin{bmatrix} \overline{Z}_{Nzw}^{S2S5} & 0 & 0 \\ 0 & \overline{Z}_{Mx\theta x}^{S2S5} & 0 \\ 0 & 0 & \overline{Z}_{My\theta y}^{S2S5} \end{bmatrix} \tag{B2,B3}$$

$$\mathbf{Z}_{21} = \begin{bmatrix} \overline{Z}_{Nzw}^{S5S2} & 0 & 0 \\ 0 & \overline{Z}_{Mx\theta x}^{S5S2} & 0 \\ 0 & 0 & \overline{Z}_{My\theta y}^{S5S2} \end{bmatrix} \qquad \mathbf{Z}_{22} = \begin{bmatrix} \overline{Z}_{Nzw}^{S5S5} & 0 & 0 \\ 0 & \overline{Z}_{Mx\theta x}^{S5S5} & 0 \\ 0 & 0 & \overline{Z}_{My\theta y}^{S5S5} \end{bmatrix} \tag{B4,B5}$$

However some care has to be taken while doing this operation. The impedance terms related to the axial velocity $\dot{w}_{Sj}$ and force N_{zSi} parameters remains the same as those of the 12×12 impedance matrix (e.g. $\overline{Z}_{Nzw}^{SiSj} = Z_{Nzw}^{SiSj}$). These four point and transfer impedances, related to longitudinal waves, are given by the following relations:

$$Z_{Nzw}^{S2S2}(\omega) = \frac{\tilde{N}_{zS2}(\omega)}{\tilde{\dot{w}}_{S2}(\omega)} = Z_{Nzw}^{S5S5}(\omega) = \frac{\tilde{N}_{zS5}(\omega)}{\tilde{\dot{w}}_{S5}(\omega)} = \frac{1}{j\omega}\frac{E_m A_m k_{lm} \lambda_1}{\lambda_2} \tag{B6}$$

$$Z_{Nzw}^{S2S5}(\omega) = \frac{\tilde{N}_{zS5}(\omega)}{\tilde{\dot{w}}_{S2}(\omega)} = Z_{Nzw}^{S5S2}(\omega) = \frac{\tilde{N}_{zS2}(\omega)}{\tilde{\dot{w}}_{S5}(\omega)} = -\frac{1}{j\omega}\frac{E_m A_m k_{lm}}{\lambda_2} \tag{B7}$$

where E_m is the Young's modulus of elasticity, A_m is the mount cross sectional area and ω is the circular frequency (rad/s). $k_{lm} = \omega/c_{lm} = \omega/\sqrt{E_m/\rho_m}$ is the longitudinal wave number, c_{lm} is the phase velocity of longitudinal waves and ρ_m is the density of the material. The two parameters λ_1 and λ_2 are given by

$$\lambda_1 = \cos k_{lm} h_m \qquad \lambda_2 = \sin k_{lm} h_m \qquad \text{(B8,B9)}$$

where h_m is the beam height.

Neglecting the angular velocity and moment in the z direction at the two ends of the mount element, θ_z and M_z respectively, implies that the two driving point and two transfer impedance terms related to torsional vibration are not accounted for in the impedance matrix of the mount element. Therefore the terms $Z_{Mz\theta z}^{SiSj}$ are set to zero and the rows and columns number 6 and 12 of the impedance matrix given in equation (B1) are taken out.

Neglecting the velocities in x and y directions, $\dot{u}$ and $\dot{v}$, and the force components N_x and N_y can not be treated so simply. In fact, in order to derive the four impedance matrices $\mathbf{Z}_{11}$, $\mathbf{Z}_{12}$, $\mathbf{Z}_{21}$ and $\mathbf{Z}_{22}$, it is not sufficient to take off the impedance terms related to those kinematic and dynamic parameters (e.g. set $Z_{Nxu}^{SiSj} = Z_{Nyv}^{SiSj} = Z_{Nx\theta y}^{SiSj} = Z_{Nyv}^{SiSj} = Z_{Mxv}^{SiSj} = Z_{Myu}^{SiSj} = 0$ and delete rows and coloumns number 1, 2, 7 and 8 of the impedance matrix given in equation (B1)).

This point is discussed by O'Hara [33] and Rubin [11], who discuss why it is not generally correct to pick out only some of the elements of a $n \times n$ impedance matrix, which relates force and velocity parameters that are coupled, in order to build up a smaller $m \times m$ impedance matrix. This is because the elements of the $n \times n$ or $m \times m$ impedance matrices are derived by imposing a "constraint" on the linear or angular velocity parameters accounted for in the matrix relation $\mathbf{f} = \mathbf{Z}\mathbf{v}$. For example, the impedance term $Z_{\theta xMx}^{S5S2}$ for the 6×6 impedance matrix is calculated assuming the following constraints:

$$Z_{Mx\theta x}^{S2S5} = \frac{\tilde{M}_{xS2}}{\tilde{\dot{\theta}}_{xS5}} \quad \text{and} \quad w_{S2} = w_{S5} = \theta_{xS2} = \theta_{yS2} = \theta_{yS5} = 0 \qquad \text{(B10)}$$

(note that no constraint is placed on u_{S2}, u_{S5}, v_{S2}, v_{S5}, θ_{zS2}, θ_{zS5} which can take any value) and for the 12×12 impedance matrix,

$$Z_{Mx\theta x}^{S2S5} = \frac{\tilde{M}_{xS2}}{\tilde{\dot{\theta}}_{xS5}} \quad \text{and} \quad u_{S2} = u_{S5} = v_{S2} = v_{S5} = w_{S2} = w_{S5} = \theta_{xS2} = \theta_{yS2} = \theta_{yS5} = \theta_{zS2} = \theta_{zS5} = 0 \qquad \text{(B11)}$$

Thus the $Z_{Mx\theta x}^{S2S5}$ term differs when calculated with either equation (B10) or (B11). This is because the one dimensional mounting element is constrained in a different way in the two cases.

If instead, a mobility relation $\mathbf{v} = \mathbf{M}\mathbf{f}$ is considered, it can be shown that the reduction from a m to a $n < m$ degrees-of-freedom mobility matrix relation can be carried out simply by "collapsing" the mobility matrix $\mathbf{M}_{m \times m}$ into the $\mathbf{M}_{n \times n}$. In fact, if the mobility term $M_{\theta xMx}^{S2S5}$ is considered, it can be noticed that whether this term is calculated for a 6×6 or a 12×12 mobility matrix (e.g. either only three or all six degrees-of-freedom are accounted for in the matrix relation) the same result is obtained since only the excitations are constrained in a different way. So for the 6×6 mobility matrix

$$M_{\theta xMx}^{S2S5} = \frac{\tilde{\dot{\theta}}_{xS5}}{\tilde{M}_{xS2}} \quad \text{and} \quad N_{zS2} = N_{zS5} = M_{xS2} = M_{ySz} = M_{yS5} = 0 \tag{B12}$$

(note that no constraint is placed on the excitation parameters N_{xS2}, N_{xS5}, N_{yS2}, N_{yS5}, M_{zS2}, M_{zS5}, although they could be implicitly assumed to be zero) and for the 12×12 mobility matrix

$$M_{\theta xMx}^{S2S5} = \frac{\tilde{\dot{\theta}}_{xS5}}{\tilde{M}_{xS2}} \quad \text{and} \quad N_{xS2} = N_{xS5} = N_{yS2} = N_{yS5} = N_{zS2} = N_{zS5} = M_{xS2} = M_{yS2} = M_{yS5} = M_{zS2} = M_{zS5} = 0 \tag{B13}$$

Therefore, the 6×6 mobility matrix $\mathbf{M}_{6\times6}$ is correct even if its elements are picked up form the 12×12 mobility matrix $\mathbf{M}_{12\times12}$.

In conclusion the reduction of a $m\times m$ impedance matrix to a smaller $n\times n$ matrix is possible only if the kinematic and dynamic parameters of the impedance relation $\mathbf{f}=\mathbf{Zv}$ are uncoupled. This is not the case for mobility matrices. It is in fact possible to reduce a $m\times m$ mobility matrix to a smaller $n\times n$ matrix without the need of recalculating the mobility terms even if the kinematic and dynamic parameters of the mobility relation $\mathbf{v}=\mathbf{Zf}$ are coupled. Therefore, for the specific case examined in this appendix, the impedance terms $\overline{Z}_{Mx\theta x}^{SjSi}$, $\overline{Z}_{My\theta y}^{SjSi}$ cannot be derived directly from the equivalent ones of the 12×12 impedance matrix of equation (B1). For their exact calculation there are two options: either they are analytically calculated assuming the pertinent boundary conditions at each end of the mount element (e.g. by constraining the $\dot{u}$ and $\dot{v}$ linear velocities and the N_x, and N_y force components) or they are calculated by inverting a reduced mobility matrix $\mathbf{M}_{6\times6}$ which has been directly derived from the complete mobility matrix $\mathbf{M}_{12\times12}$ which refers to all six kinematic and dynamic parameters at each end of the mount element.

However, there is a second problem that has to be considered before moving on to calculate the impedance terms $\overline{Z}_{Mx\theta x}^{SjSi}$ and $\overline{Z}_{My\theta y}^{SjSi}$. Flexural waves in a beam, unlike the other wave types, are represented by four field parameters instead of two [31]. For example the flexural vibration in the *x*-*z* plane is represented by the linear velocity and force in *x* direction, $\dot{u}$ and N_x, and the angular velocity and moment in *y* direction, $\dot{\theta}_y$ and M_y. These four variables are coupled so that the angular velocity $\dot{\theta}_y$ at one end of the mount element, let us say junction S_2, due to a collocated moment M_y can be found only if the linear velocity $\dot{u}$ and force N_x at the two ends are fixed and if the angular velocity and moment in *y* direction, $\dot{\theta}_y$ and M_y, at the opposite end of the one where the angular velocity is determined, junction S_5, are specified. Therefore, even when the mobility matrix for the reduced case accounting for three degrees-of-freedom at each end of the mount is calculated, in order to derive the mobility term $\overline{M}_{\theta yMy}^{S2S2} = \dot{\theta}_{yS2} / M_{yS2j}\big|_{M_{yS5}=0}$, the values of the linear velocity $\dot{u}$ and force N_x at the two ends has to be specified. The boundary conditions for the angular velocity $\dot{\theta}_y$ and moment M_y at the junction S_5 are set to be as those of a freely suspended beam so that $\dot{\theta}_{yS5} \neq 0$ and $M_{yS5} = 0$. The other four boundary conditions requires some thought before they are fixed. They are in fact neglected in the formulation of the problem (see section 4). The problem is to transform the verb " to neglect" into a mathematical expression.

Indeed there are four possible choices for the linear velocity $\dot{u}$ and force N_x at the two ends of the mount element: first $\dot{u}_{Sj}=0$ and $N_{xSj}=0$; second, $\dot{u}_{Sj}\neq 0$ and $N_{xSj}\neq 0$; third, $\dot{u}_{Sj}=0$ and $N_{xSj}\neq 0$ and fourth $\dot{u}_{Sj}\neq 0$ and $N_{xSj}=0$. The first two can not be imposed since the solution of the wave equation would be undetermined. The third and the fourth one are instead compatible with the flexural wave equation and, when associated to the boundary condition chosen for the angular velocity and moment at the two ends, they give rise to the study of either a freely suspended beam whose boundary conditions at the two ends are $\dot{\theta}_{ySS}\neq 0$, $M_{xS5}=0$, $\dot{u}_{S2}\neq 0$ and $N_{xS2}=0$ or the study of a pinned - pinned beam having instead the following boundary conditions at the two ends $\dot{\theta}_{ySS}\neq 0$, $M_{ySj}=0$, $\dot{u}_{Sj}=0$ and $N_{xSj}\neq 0$.

In view of the above mentioned problem about the reduction of the number of rows and culums of an impedance matrix, the impedance terms $\overline{Z}^{SjSi}_{MxOx}$, $\overline{Z}^{SjSi}_{MyOy}$ have been derived by inverting the mobility matrix given in to the following expression:

$$\begin{Bmatrix} \dot{w}_{S2} \\ \dot{\theta}_{xS2} \\ \dot{\theta}_{yS2} \\ \dot{w}_{S5} \\ \dot{\theta}_{xS5} \\ \dot{\theta}_{yS5} \end{Bmatrix} = \begin{bmatrix} M^{S2S2}_{wNz} & 0 & 0 & M^{S2S5}_{wNz} & 0 & 0 \\ 0 & M^{S2S2}_{\theta xMx} & 0 & 0 & M^{S2S5}_{\theta xMx} & 0 \\ 0 & 0 & M^{S2S2}_{\theta yMy} & 0 & 0 & M^{S2S5}_{\theta yMy} \\ M^{S5S2}_{wNz} & 0 & 0 & M^{S5S5}_{wNz} & 0 & 0 \\ 0 & M^{S5S2}_{\theta yMy} & 0 & 0 & M^{S5S5}_{\theta xMx} & 0 \\ 0 & 0 & M^{S5S2}_{\theta xMx} & 0 & 0 & M^{S5S5}_{\theta yMy} \end{bmatrix} \begin{Bmatrix} N_{zS2} \\ M_{xS2} \\ M_{yS2} \\ N_{zS5} \\ M_{xS5} \\ M_{yS5} \end{Bmatrix} \tag{B14}$$

This 6×6 mobility matrix has been derived exactly by cancelling row and columns number 1, 2, 6, 7, 8 and 12 of the complete 12×12 mobility matrix assuming the mount element freely suspended:

$$\begin{Bmatrix} N_{xS2} \\ N_{yS2} \\ N_{zS2} \\ M_{xS2} \\ M_{yS2} \\ M_{zS2} \\ N_{xS5} \\ N_{yS5} \\ N_{zS5} \\ M_{xS5} \\ M_{yS5} \\ M_{zS5} \end{Bmatrix} = \begin{bmatrix} M^{S2S2}_{uNx} & 0 & 0 & 0 & M^{S2S2}_{\theta yNx} & 0 & M^{S2S5}_{uNx} & 0 & 0 & 0 & M^{S2S5}_{\theta yNx} & 0 \\ 0 & M^{S2S2}_{vNy} & 0 & M^{S2S2}_{\theta xNy} & 0 & 0 & 0 & M^{S2S5}_{vNy} & 0 & M^{S2S5}_{\theta xNy} & 0 & 0 \\ 0 & 0 & M^{S2S2}_{wNz} & 0 & 0 & 0 & 0 & 0 & M^{S2S5}_{wNz} & 0 & 0 & 0 \\ 0 & M^{S2S2}_{vMx} & 0 & M^{S2S2}_{\theta xMx} & 0 & 0 & 0 & M^{S2S5}_{vMx} & 0 & M^{S2S5}_{\theta xMx} & 0 & 0 \\ M^{S2S2}_{uMy} & 0 & 0 & 0 & M^{S2S2}_{\theta yMy} & 0 & M^{S2S5}_{uMy} & 0 & 0 & 0 & M^{S2S5}_{\theta yMy} & 0 \\ 0 & 0 & 0 & 0 & 0 & M^{S2S2}_{\theta zMz} & 0 & 0 & 0 & 0 & 0 & M^{S2S5}_{\theta zMz} \\ M^{S5S2}_{uNx} & 0 & 0 & 0 & M^{S5S2}_{\theta yNx} & 0 & M^{S5S5}_{uNx} & 0 & 0 & 0 & M^{S5S5}_{\theta yNx} & 0 \\ 0 & M^{S5S2}_{vNy} & 0 & M^{S5S2}_{\theta xNy} & 0 & 0 & 0 & M^{S5S5}_{vNy} & 0 & M^{S5S5}_{\theta yNy} & 0 & 0 \\ 0 & 0 & M^{S5S2}_{wNz} & 0 & 0 & 0 & 0 & 0 & M^{S5S5}_{wNz} & 0 & 0 & 0 \\ 0 & M^{S5S2}_{vMx} & 0 & M^{S5S2}_{\theta xMx} & 0 & 0 & 0 & M^{S5S5}_{vMx} & 0 & M^{S5S5}_{\theta xMx} & 0 & 0 \\ M^{S5S2}_{uMy} & 0 & 0 & 0 & M^{S5S2}_{\theta yMy} & 0 & M^{S5S5}_{uMy} & 0 & 0 & 0 & M^{S5S5}_{\theta yMy} & 0 \\ 0 & 0 & 0 & 0 & 0 & M^{S5S2}_{\theta zMz} & 0 & 0 & 0 & 0 & 0 & M^{S5S5}_{\theta zMz} \end{bmatrix} \begin{Bmatrix} \dot{u}_{S2} \\ \dot{v}_{S2} \\ \dot{w}_{S2} \\ \dot{\theta}_{xS2} \\ \dot{\theta}_{yS2} \\ \dot{\theta}_{zS2} \\ \dot{u}_{S5} \\ \dot{v}_{S5} \\ \dot{w}_{S5} \\ \dot{\theta}_{xS5} \\ \dot{\theta}_{yS5} \\ \dot{\theta}_{zS5} \end{Bmatrix} \tag{B15}$$

All the mobility terms of this mobility matrix can be found on page 363, table 7.1(c), of Bishop and Johnson [32].

With reference to the other problem discussed above, it has been decided to also calculate the impedance terms $\overline{Z}^{SjSi}_{MxOx}$, $\overline{Z}^{SjSi}_{MyOy}$ for a beam element with both ends pinned in x and y directions. The same procedure has been followed as for the case of a freely suspended element. First, the reduced 6×6 mobility matrix has been

derived for a mount element with each end pinned in x and y directions and second, this mobility matrix has been inverted in order to give the equivalent impedance matrix with the exact $\overline{Z}^{SjSi}_{Mx\theta x}$, $\overline{Z}^{SjSi}_{My\theta y}$ impedance terms.

With reference to the freely suspended boundary condition (e.g. $\dot{u}_{Sj} \neq 0$, $\dot{v}_{Sj} \neq 0$, $\dot{\theta}_{xSj} \neq 0$, $\dot{\theta}_{ySj} \neq 0$ and $N_{xSj} = 0$, $N_{ySj} = 0$, $M_{xSj} = 0$, $M_{ySj} = 0$) the eight impedance elements have been calculated as follows:

$$Z^{S2S2}_{Mx\theta x}(\omega) = \frac{\tilde{M}_{xS2}(\omega)}{\dot{\tilde{\theta}}_{xS2}(\omega)} = Z^{S5S5}_{Mx\theta x}(\omega) = \frac{\tilde{M}_{xS5}(\omega)}{\dot{\tilde{\theta}}_{xS5}(\omega)} = \frac{1}{j\omega}\frac{E_m I_m k_{fm} \varphi_3 \varphi_6}{\varphi_6^2 - \varphi_7^2} \; ; \tag{B16}$$

$$Z^{S2S2}_{My\theta y}(\omega) = \frac{\tilde{M}_{yS2}(\omega)}{\dot{\tilde{\theta}}_{yS2}(\omega)} = Z^{S5S5}_{My\theta y}(\omega) = \frac{\tilde{M}_{yS5}(\omega)}{\dot{\tilde{\theta}}_{yS5}(\omega)} = -\frac{1}{j\omega}\frac{E_m I_m k_{fm} \varphi_3 \varphi_7}{\varphi_6^2 - \varphi_7^2} \; ; \tag{B17}$$

$$Z^{S2S5}_{Mx\theta x}(\omega) = \frac{\tilde{M}_{xS2}(\omega)}{\dot{\tilde{\theta}}_{xS5}(\omega)} = Z^{S5S2}_{Mx\theta x}(\omega) = \frac{\tilde{M}_{xS5}(\omega)}{\dot{\tilde{\theta}}_{xS2}(\omega)} = -\frac{1}{j\omega}\frac{E_m I_m k_{fm} \varphi_3 \varphi_7}{\varphi_6^2 - \varphi_7^2} \; ; \tag{B18}$$

$$Z^{S2S5}_{My\theta y}(\omega) = \frac{\tilde{M}_{yS2}(\omega)}{\dot{\tilde{\theta}}_{yS5}(\omega)} = Z^{S5S2}_{My\theta y}(\omega) = \frac{\tilde{M}_{yS5}(\omega)}{\dot{\tilde{\theta}}_{yS2}(\omega)} = \frac{1}{j\omega}\frac{E_m I_m k_{fm} \varphi_3 \varphi_6}{\varphi_6^2 - \varphi_7^2} \; . \tag{B19}$$

where

$$\varphi_3 = \cos k_{fm} h_m \cosh k_{fm} h_m - 1 \tag{B20}$$

$$\varphi_6 = \cos k_{fm} h_m \sinh k_{fm} h_m + \sin k_{fm} h_m \cosh k_{fm} h_m \tag{B21}$$

$$\varphi_7 = \sin k_{fm} h_m + \sinh k_{fm} h_m \tag{B22}$$

and $k_{fm} = \omega / c_{fm} = \sqrt[4]{\omega^2 m'/B}$ is the flexural wave number, $c_{fm} = \sqrt[2]{\omega}\sqrt[4]{B/m'}$ is the phase velocity of flexural waves, $B = E_m I_m$ is the bending stiffness of the mount, $I_m = I_x = I_y = \pi a_m^4 / 4$ is the area moment of inertia of the circular mount cross section with radius a, $m' = \rho_m A_m$ is the density per unit area of the material.

With reference to the pinned in x and y directions boundary condition (e.g. $\dot{u}_{Sj} = 0$, $\dot{v}_{Sj} = 0$, $\dot{\theta}_{xSj} \neq 0$, $\dot{\theta}_{ySj} \neq 0$, and $N_{xSj} = 0$, $N_{ySj} = 0$, $M_{xSy} = 0$, $M_{ySy} = 0$) the eight impedance elements have been calculated as follows:

$$Z^{S2S2}_{Mx\theta x}(\omega) = \frac{\tilde{M}_{xS2}(\omega)}{\dot{\tilde{\theta}}_{xS2}(\omega)} = Z^{S5S5}_{Mx\theta x}(\omega) = \frac{\tilde{M}_{xS5}(\omega)}{\dot{\tilde{\theta}}_{xS5}(\omega)} = \frac{2}{j\omega}\frac{E_m I_m k_{fm} \varphi_1 \varphi_5}{\varphi_5^2 - \varphi_8^2} \; ; \tag{B23}$$

$$Z_{My\theta y}^{S2S2}(\omega)=\frac{\tilde{M}_{yS2}(\omega)}{\dot{\tilde{\theta}}_{yS2}(\omega)}=Z_{My\theta y}^{S5S5}(\omega)=\frac{\tilde{M}_{yS5}(\omega)}{\dot{\tilde{\theta}}_{yS5}(\omega)}=-\frac{2}{j\omega}\frac{E_m I_m k_{fm}\varphi_1\varphi_8}{\varphi_5^2-\varphi_8^2}\ ; \tag{B24}$$

$$Z_{Mx\theta x}^{S2S5}(\omega)=\frac{\tilde{M}_{xS2}(\omega)}{\dot{\tilde{\theta}}_{xS5}(\omega)}=Z_{Mx\theta x}^{S5S2}(\omega)=\frac{\tilde{M}_{xS5}(\omega)}{\dot{\tilde{\theta}}_{xS2}(\omega)}=-\frac{2}{j\omega}\frac{E_m I_m k_{fm}\varphi_1\varphi_8}{\varphi_5^2-\varphi_8^2}\ ; \tag{B25}$$

$$Z_{My\theta y}^{S2S5}(\omega)=\frac{\tilde{M}_{yS2}(\omega)}{\dot{\tilde{\theta}}_{yS5}(\omega)}=Z_{My\theta y}^{S5S2}(\omega)=\frac{\tilde{M}_{yS5}(\omega)}{\dot{\tilde{\theta}}_{yS2}(\omega)}=\frac{2}{j\omega}\frac{E_m I_m k_{fm}\varphi_1\varphi_5}{\varphi_5^2-\varphi_8^2}\ . \tag{B26}$$

where

$$\varphi_1=\sin k_{fm}h_m \sinh k_{fm}h_m \tag{B27}$$

$$\varphi_5=\cos k_{fm}h_m \sinh k_{fm}h_m-\sin k_{fm}h_m \cosh k_{fm}h_m \tag{B28}$$

$$\varphi_8=\sin k_{fm}h_m-\sinh k_{fm}h_m \tag{B29}$$

Therefore two set of impedance terms $\overline{Z}_{Mx\theta x}^{SjSi}$ and $\overline{Z}_{My\theta y}^{SjSi}$ have been calculated for the impedance matrices $\mathbf{Z}_{11}$, $\mathbf{Z}_{12}$, $\mathbf{Z}_{21}$ and $\mathbf{Z}_{22}$ to be used into equations (55) and (56).

The results obtained with the two sets of impedance matrices have been compared with measured data (as in section 5.5) in order to estimate which one between the freely suspended and the pinned in *x* and *y* directions boundary conditions is the most representative one for the system studied in this report.

The comparison has been carried out for the two plate system shown in figure 2 having either a rubber or aluminium mount with lumped masses at the top and bottom ends ($W_t=9.8\times10^{-3}$ Kg $W_b=3.1\times10^{-3}$ Kg) and with inertial control actuators acting at the top end of the mounts. The control strategy considered is the cancellation of axial velocities at the top of the mounts. The primary excitation has been chosen at position P_3. Figures B3 and B4 shows the estimate of the receiver K_{Er} kinetic energy without (top plot) and with (bottom plot) active control for the isolator systems with rubber mounts when the four impedance matrices $\mathbf{Z}_{11}$, $\mathbf{Z}_{12}$, $\mathbf{Z}_{21}$ and $\mathbf{Z}_{22}$ have been calculated for a freely suspended or pinned mount element. Figures B5 and B6 shows the same type of plots but for the case where the four impedance matrices $\mathbf{Z}_{11}$, $\mathbf{Z}_{12}$, $\mathbf{Z}_{21}$ and $\mathbf{Z}_{22}$ have been calculated for an aluminium mount element.

From these plots it can be seen that when there are no control forces the results obtained with either types of impedance matrix are very good. When the control forces are active result which line up best with the experimental data are achieved when the four impedance matrices $\mathbf{Z}_{11}$, $\mathbf{Z}_{12}$, $\mathbf{Z}_{21}$ and $\mathbf{Z}_{22}$ are calculated for a freely suspended mount.

In view of these results it has been chosen to present in this report the results obtained by using the matrix model with the four impedance matrices $\mathbf{Z}_{11}$, $\mathbf{Z}_{12}$, $\mathbf{Z}_{21}$ and $\mathbf{Z}_{22}$ calculated for a freely suspended mount.

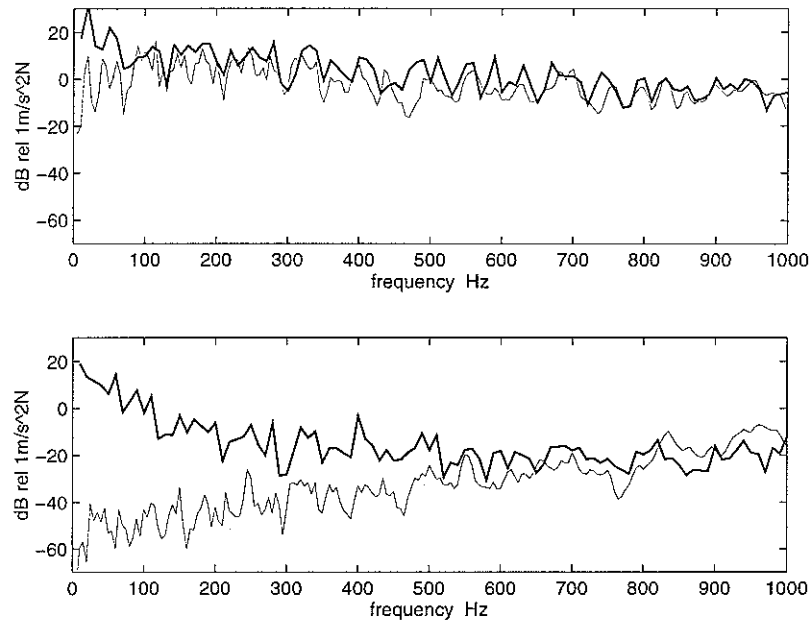

Figure B3: Estimate of the receiver K_{Er} kinetic energy without (top plot) and with (bottom plot) active control of the out-of-plane velocities at the receiver mounts junction when the primary force F_{p3} is exciting the two panel system with three rubber mounts having block masses at the ends. Solid line: experimental predictions, faint line: simulations assuming the mount element freely suspended.

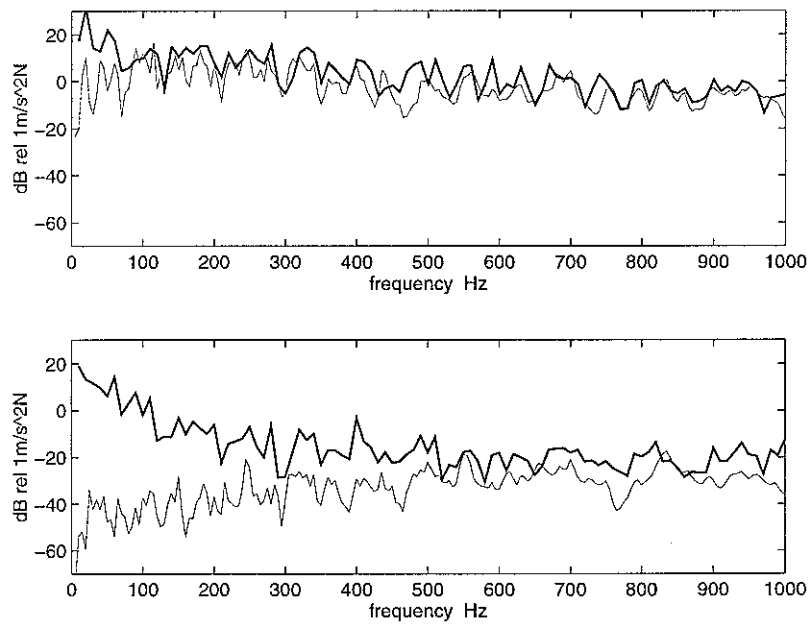

Figure B4: Estimate of the receiver K_{Er} kinetic energy without (top plot) and with (bottom plot) active control of the out-of-plane velocities at the receiver mounts junction when the primary force F_{p3} is exciting the two panel system with three rubber mounts having block masses at the ends. Solid line: experimental predictions, faint line: simulations assuming the mount element pinned in x and y directions.

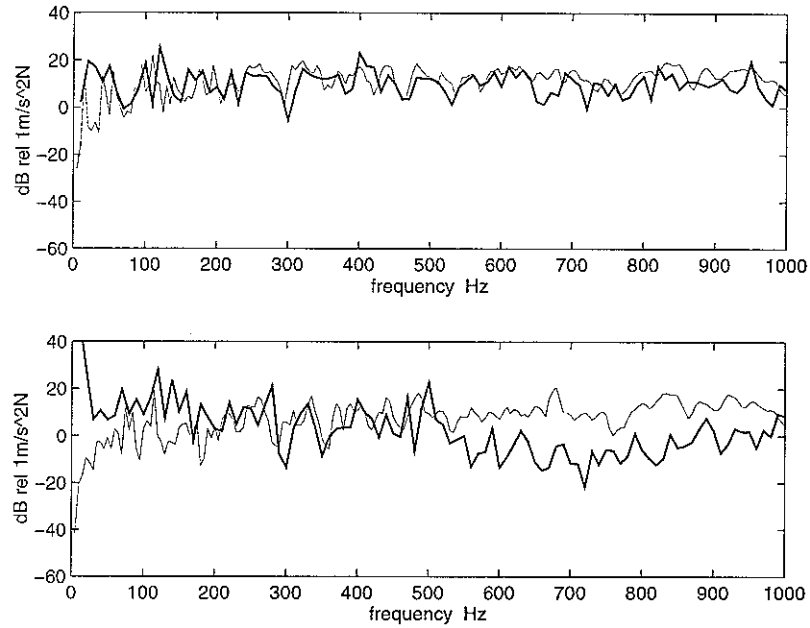

Figure B5: Estimate of the receiver K_{Er} kinetic energy without (top plot) and with (bottom plot) active control of the out-of-plane velocities at the receiver mounts junction when the primary force F_{p3} is exciting the two panel system with three aluminium mounts having block masses at the ends. Solid line: experimental predictions, faint line: simulations assuming the mount element freely suspended.

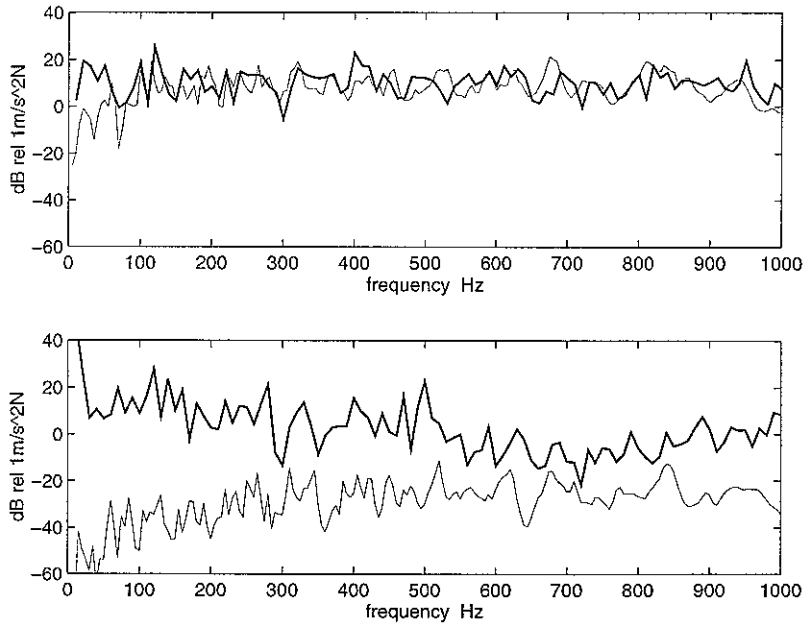

Figure B6: Estimate of the receiver K_{Er} kinetic energy without (top plot) and with (bottom plot) active control of the out-of-plane velocities at the receiver mounts junction when the primary force F_{p3} is exciting the two panel system with three aluminium mounts having block masses at the ends. Solid line: experimental predictions, faint line: simulations assuming the mount element pinned in x and y directions.

If the inertial effects due to the components used to connect the mounting system to the plates and to connect force and velocity sensors at the top of the mounts are also accounted and modelled as a pair of rectangular parallelepiped block masses connected at the mounts ends, the four impedance matrices $\mathbf{Z}_{11}$, $\mathbf{Z}_{12}$, $\mathbf{Z}_{21}$ and $\mathbf{Z}_{22}$ assume the following form:

$$\mathbf{Z}_{11} = \begin{bmatrix} Z_{Nzw}^{S2S2} + j\omega W & 0 & 0 \\ 0 & Z_{M\theta x}^{S2S2} + j\omega I_x & 0 \\ 0 & 0 & Z_{M\theta y}^{S2S2} + j\omega I_y \end{bmatrix} \qquad \mathbf{Z}_{12} = \begin{bmatrix} Z_{Nzw}^{S2S5} & 0 & 0 \\ 0 & Z_{M\theta x}^{S2S5} & 0 \\ 0 & 0 & Z_{M\theta y}^{S2S5} \end{bmatrix} \qquad \text{(B30,B31)}$$

$$\mathbf{Z}_{21} = \begin{bmatrix} Z_{Nzw}^{S5S2} & 0 & 0 \\ 0 & Z_{M\theta x}^{S5S2} & 0 \\ 0 & 0 & Z_{M\theta y}^{S5S2} \end{bmatrix} \qquad \mathbf{Z}_{22} = \begin{bmatrix} Z_{Nzw}^{S5S5} + j\omega W & 0 & 0 \\ 0 & Z_{M\theta x}^{S5S5} + j\omega I_x & 0 \\ 0 & 0 & Z_{M\theta y}^{S5S5} + j\omega I_y \end{bmatrix}. \qquad \text{(B32,B33)}$$

where W is the weight of the top or bottom block masses, I_x and I_y are the mass moment of inertia with reference to the x and y axis of the system of reference placed at the mount ends.

The excitation matrices $\mathbf{V}_m$ used in equations (55) or (56) relates the force and moment parameters at the mounts junctions to the single inertial control axial force or the pair of reactive axial forces acting on each mount. As shown in figure B1 the reactive or inertial control excitation are modelled as acting at each end of the mounts so that the excitations sub-matrix V_I has the following form:

$$\mathbf{V}_1 = \begin{bmatrix} 1 \\ 0 \\ 0 \end{bmatrix}. \qquad \text{(B34)}$$